JGR Biogeosciences

RESEARCH ARTICLE
10.1029/2021JG006485

Effects of Reversal of Water Flow in an Arctic Floodplain River on Fluvial Emissions of CO_2 and CH_4

K. Castro-Morales[1], A. Canning[2], A. Körtzinger[2,3], M. Göckede[4], K. Küsel[1,5], W. A. Overholt[1], T. Wichard[6], S. Redlich[6], S. Arzberger[1,7], O. Kolle[4], and N. Zimov[8]

[1]Friedrich-Schiller University Jena, Institute of Biodiversity, Jena, Germany, [2]GEOMAR Helmholtz Centre for Ocean Research Kiel, Kiel, Germany, [3]Christian Albrecht University Kiel, Kiel, Germany, [4]Max Planck Institute for Biogeochemistry, Jena, Germany, [5]German Centre for Integrative Biodiversity Research (iDiv) Halle-Jena-Leipzig, Leipzig, Germany, [6]Friedrich-Schiller University Jena, Institute for Inorganic and Analytical Chemistry, Jena, Germany, [7]Now at University of Bayreuth, Bayreuth, Germany, [8]Pleistocene Park, Northeast Science Station, Chersky, Russia

Key Points:

- Elevated concentration and fluxes of carbon dioxide and methane in Ambolikha River decrease from the late freshet to summer
- Total floodplain methane emissions were higher than the methane emitted from Ambolikha River
- Hydraulic connectivity and river flow reversals in Arctic streams can affect C replenishment and emissions

Supporting Information:

Supporting Information may be found in the online version of this article.

Correspondence to:

K. Castro-Morales,
karel.castro.morales@uni-jena.de

Citation:

Castro-Morales, K., Canning, A., Körtzinger, A., Göckede, M., Küsel, K., et al. (2022). Effects of reversal of water flow in an Arctic floodplain river on fluvial emissions of CO_2 and CH_4. *Journal of Geophysical Research: Biogeosciences*, *127*, e2021JG006485. https://doi.org/10.1029/2021JG006485

Received 14 JUN 2021
Accepted 18 DEC 2021

Author Contributions:

Conceptualization: K. Castro-Morales, M. Göckede
Data curation: K. Castro-Morales, A. Canning, M. Göckede, W. A. Overholt, T. Wichard, S. Redlich, S. Arzberger
Formal analysis: K. Castro-Morales
Funding acquisition: K. Castro-Morales, A. Körtzinger, M. Göckede, K. Küsel
Investigation: K. Castro-Morales, A. Körtzinger, M. Göckede, K. Küsel, W. A. Overholt, T. Wichard
Methodology: K. Castro-Morales, A. Canning, A. Körtzinger, M. Göckede, K. Küsel, W. A. Overholt, T. Wichard, O. Kolle, N. Zimov

Abstract When organic matter from thawed permafrost is released, the sources and sinks of greenhouse gases (GHGs), like carbon dioxide (CO_2) and methane (CH_4) in Arctic rivers will be influenced in the future. However, the temporal variation, environmental controls, and magnitude of the Arctic riverine GHGs are largely unknown. We measured in situ high temporal resolution concentrations of CO_2, CH_4, and oxygen (O_2) in the Ambolikha River in northeast Siberia between late June and early August 2019. During this period, the largely supersaturated riverine CO_2 and CH_4 concentrations decreased steadily by 90% and 78%, respectively, while the O_2 concentrations increased by 22% and were driven by the decreasing water temperature. Estimated gas fluxes indicate that during late June 2019, significant emissions of CO_2 and CH_4 were sustained, possibly by external terrestrial sources during flooding, or due to lateral exchange with gas-rich downstream-flowing water. In July and early August, the river reversed its flow constantly and limited the water exchange at the site. The composition of dissolved organic matter and microbial communities analyzed in discrete samples also revealed a temporal shift. Furthermore, the cumulative total riverine CO_2 emissions (36.8 gC-CO_2 m^{-2}) were nearly five times lower than the CO_2 uptake at the adjacent floodplain. Emissions of riverine CH_4 (0.21 gC-CH_4 m^{-2}) were 16 times lower than the floodplain CH_4 emissions. Our study revealed that the hydraulic connectivity with the land in the late freshet, and reversing flow directions in Arctic streams in summer, regulate riverine carbon replenishment and emissions.

Plain Language Summary When the snow and ice melt in the Arctic, then organic matter, carbon dioxide (CO_2), and methane (CH_4) can be transported from land into rivers. Bacteria or sunlight transform river organic matter, releasing more of those gases. However, little is known about how CO_2 and CH_4 levels in Arctic rivers change over time or how environmental factors affect them. We measured CO_2, CH_4, and oxygen in the Ambolikha River in northeast Siberia, from late June to early August 2019. Riverine CO_2 and CH_4 concentrations decreased over time but remained high enough to be emitted into the atmosphere. Riverine CO_2 emissions were five times lower than floodplain terrestrial plant CO_2 uptake. Riverine CH_4 emissions were 16 times lower than floodplain emissions. Upstream fluvial contributions and lateral influences from the floodplain, must have maintained high riverine gas concentrations during flooding. The direction of the river's flow reversed repeatedly in July and early August, limiting water and gas exchange. Changes in river flow patterns and permafrost thaw must be considered to better quantify temporal and spatial variations in Arctic riverine CO_2 and CH_4 emissions. This will help us understand the role of Arctic aquatic ecosystems in regional and global carbon budgets.

1. Introduction

Rivers connect the land with oceans and are effective active pipes where terrestrial carbon undergoes numerous transformations (Cole et al., 2007). The majority of the carbon in rivers and streams is emitted into the atmosphere as carbon dioxide (CO_2) (Raymond et al., 2013) and methane (CH_4) (Stanley et al., 2016). Thus, it is estimated that less than 50% (~0.9 PgC yr^{-1}) of the total carbon export from global inland waters (1.9–3.2 PgC yr^{-1}) reaches the oceans (Abril & Borges, 2019).

Resources: K. Castro-Morales, A. Körtzinger, M. Göckede, K. Küsel
Supervision: K. Castro-Morales, A. Körtzinger, K. Küsel, T. Wichard
Writing – original draft: K. Castro-Morales
Writing – review & editing: K. Castro-Morales, A. Canning, A. Körtzinger, M. Göckede, K. Küsel, W. A. Overholt, T. Wichard, S. Redlich

The discharge of the six major Arctic rivers (i.e., Yenisey, Lena, Ob, Mackenzie, Yukon, and Kolyma) to the Arctic Ocean accounts for about 11% of the global total riverine discharge (Shiklomanov et al., 2000), and this discharge is increasing due to climate variations (Connolly et al., 2020; Fichot et al., 2013). In addition, rising atmospheric temperatures in this region promote the thawing of permafrost, leading to higher emission rates of CO_2 and CH_4 from land and inland waters (Meredith et al., 2019; Schuur et al., 2015; Turetsky et al., 2020). The carbon gases (C-gases) CO_2 and CH_4, are products of aerobic and anaerobic carbon degradation processes. These gases are released into the atmosphere from the seasonal unfrozen soil column (i.e., active layer) of the permafrost soil in the Arctic terrestrial ecosystems and may also be diffused into the Arctic river network via surface water runoff and groundwater (Connolly et al., 2020). The sources of C-gases from Arctic inland waters in northeast Siberia have mostly been linked to the degradation of modern carbon (Dean et al., 2020). However, the degradation of Holocene and Late Pleistocene ice and organic-rich Yedoma deposits (Schuur et al., 2015; Strauss et al., 2017) is another significant source of C-gases in the Arctic. This ancient organic matter (OM) becomes available to the Arctic rivers and streams via the thermal-erosion of permafrost soils and the collapse of shelves and river banks (Fritz et al., 2017).

The hydrologic connectivity between terrestrial and aquatic ecosystems plays a determinant role in transporting carbon compounds into fluvial networks (Covino, 2017; Pringle, 2003). Nearly 60% of the total annual dissolved organic carbon (DOC) exported to the ocean via the Arctic rivers occurs during the high-flow freshet period at the peak of snow and ice melting (May and June) (Raymond et al., 2007). This is due to the fact that during the freshet, the annual floods improve the hydrologic connectivity of small Arctic streams in the river network, as well as the mobilization of terrestrial DOC and particulate organic carbon (POC) from the active layer (Mann et al., 2012; Vonk et al., 2015). Notably, the dissolved organic matter (DOM) from permafrost (P-DOM) is highly labile compared to the bulk river and contemporary DOM (Mann et al., 2012; Spencer et al., 2015).

The production rate of CO_2 due to the photomineralization of P-DOM in soils is twice the degradation rate of contemporary DOC (Bowen et al., 2020). Thus, within a week of release, a large portion of the permafrost-derived POC: DOC ratio can be degraded to lighter chemical compounds via photochemical oxidation or bacterial biomineralization (Cory et al., 2014; Spencer et al., 2015; Stubbins et al., 2017). This lighter organic material is further transformed into CO_2 and CH_4 and transported through the Arctic fluvial network or released locally into the atmosphere.

Changes in water discharge play a critical role in the variation of CO_2 concentrations and emissions in rivers and streams, with higher emission rates occurring at higher discharge (Liu & Raymond, 2018). Contrary to main stems of rivers and large tributaries, the concentration of C-gases in Arctic inland waters, such as ponds and small streams, is generally higher than their concentration at equilibrium with the atmosphere (i.e., supersaturation) (Dean et al., 2020; Denfeld et al., 2013; Hotchkiss et al., 2015; Kling et al., 1991, 1992; Raymond et al., 2012; Striegl et al., 2012). The global cross-ecosystem carbon fluxes between terrestrial and aquatic ecosystems are largely uncertain (Abril & Borges, 2019; Karlsson et al., 2021; Regnier et al., 2013; Ward et al., 2017). In the Arctic, the significant emissions of C-gases from Arctic inland waters indicate their crucial contribution to the permafrost climate feedback and the Arctic carbon budget (Harmon, 2020; Schuur et al., 2015; Turetsky et al., 2020; Vonk et al., 2013). Nevertheless, the magnitude and spatiotemporal variability of dissolved C-gases in small Arctic streams during seasonal transitions is poorly known, due to the scarcity of continuous highly resolved direct measurements. Additionally, the relationship between the variations in C-gas concentrations and emissions in Arctic rivers and the contrasting discharge from freshet high-flow to summer low-flow is also unclear and needs further research. We expect that a large portion of the concentration of C-gases in Arctic streams is from the terrestrial origin (Connolly et al., 2020; Harms et al., 2020) and may hold a large spatiotemporal variability during seasonal transitions. To investigate this, we assessed the temporal variations and associated environmental drivers of the concentrations and fluxes of CO_2, CH_4, and O_2 in an Arctic floodplain river. High temporal resolution concentrations of these gases and other optical properties, were measured from the late freshet (end of June) until summer (early August) in 2019 in Ambolikha River, which is a tributary stream, associated to a floodplain, of the Kolyma River in northeast Siberia. Because the hydraulic connectivity between the Ambolikha River channel and the floodplain is enhanced in this area during high-flow periods, we were able to examine the relationship between the measured riverine gases at the Ambolikha River and the changes in the flow regime over time. We also compared the riverine CO_2 and CH_4 emissions with land fluxes measured at a site in the adjacent

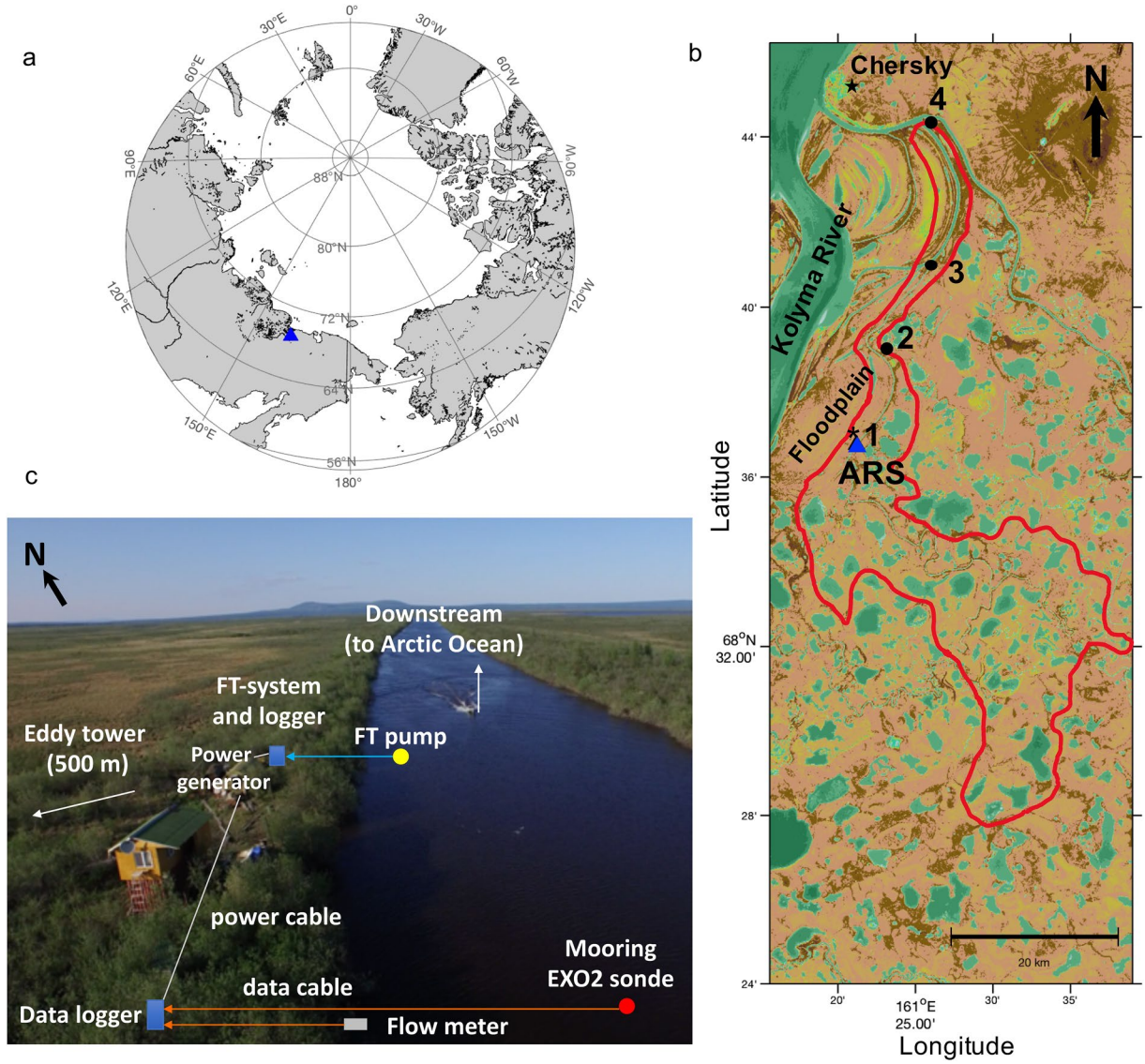

Figure 1. Location of the study area and instrumentation. Map of Northeast Siberia (a) showing the study area within (b) the Ambolikha watershed (area 121 km^2) delimited by the red line, and the location of the Ambolikha River site (ARS) for water measurements (blue triangle) and of the eddy tower (black asterisk) within the adjacent wet tussock tundra located 15 km south of Chersky (black star). Sampling points 1 at ARS, to point 4 at the Pantheleika-Ambolikha confluence (filled black markers), (c) position of the instrumentation at the ARS indicating the location of the three instruments installed at the river for continuous measurements of gases and water properties (yellow and red circles, and blue squares at the bank), and water discharge (gray rectangle). Water was pumped for CO_2 and CH_4 measurements through a pipe positioned at the blue arrow location. Schematics on the position of the data and power cables (to the power generator) are shown with orange and white lines. The Eddy tower is located 500 m inland to the west of the ARS.

wet tussock tundra (floodplain). To understand the source of these gases, we characterized the composition of microbial communities and DOM in discrete water samples collected at the start and end of the study period.

2. Methods

2.1. Ambolikha River and Its Floodplain System

The water measurements took place at a site (referred as to Ambolikha River Site or ARS hereinafter) with the geographical position of 68° 36' 46.73" N and 161° 21' 9.54" E, and located at the center of the main channel of the Ambolikha River at about 20 km upstream of the city of Chersky, Sakha Republic in northeast Siberia (Figure 1). We chose this stream for our study because of the availability of infrastructure (power generator) for

the installation of the instruments and its vicinity to the floodplain that is continuously monitored for land gas emissions. The Ambolikha River is a second-order tributary of the Kolyma River, with an estimated surface area of 1.1 km^2 (Denfeld et al., 2013). The Ambolikha watershed covers an area of ∼121 km^2 (Broderick et al., 2015) (Figure 1b) and is entirely underlain by continuous permafrost with evidence of riverbank erosion. This watershed is part of the Pantheleika-Ambolikha watershed (total area of 1,849 km^2), and has a mostly flat terrain with the highest elevations reaching 40 m above sea level and numerous thermokarst lakes and small streams (Broderick et al., 2015). The watershed delineation in Figure 1b is an approximation due to the very flat nature of the floodplain. The vast majority of the Kolyma River and its tributaries are frozen in winter and melt during late May, triggering the freshet period characterized by a rapid surge in the water discharge and floods that connect the land with the river. Discharge records from 1999 to 2019 at the Kolymsk-1 gauge station (68° 43' 48" N, 158° 43' 12" E) on the Kolyma River (Shiklomanov et al., 2020), show that the start of the freshet has shifted back over time from early June to the middle of May due to warmer and shorter winter periods. Because of the low elevations of the Ambolikha River watershed, this river becomes part of the floodplain channel system connecting to the Kolyma River main channel at the peak of the freshet. Therefore, the large temporal changes in the Kolyma River discharge can potentially influence the water flow at the ARS. The land gas emissions took place in a wet tussock tundra site that is part of an active floodplain located next to the ARS. Thus, during the freshet, the connection between the Ambolikha River and the land is enhanced via this area. This floodplain is also bounded by numerous lakes located in the north and southern areas. The study period spanned 38 days from 26 June 2019 to 2 August 2019, during the open water season at the late freshet and at the decreasing phase of the peak discharge in Kolyma River (supporting text S.1.1. and Figure S1 in Supporting Information S1).

2.2. Water Measurements

Our water measurements at the ARS followed an Eulerian approach for the flow of fluids, three instruments were installed to continuously monitor the water properties at the ARS (Figure 1c):

1. **Optical and other water properties.** An EXO2 Multiparameter sonde (YSI Inc., Xylem Inc., Yellow Springs, OH, USA) with optical and other sensors, was mounted inside a metal frame suspended in a mooring with a floating buoy above the instrument, and an anchor weight at the bottom to keep the instrument positioned at the ARS. During the entire study period, the sonde remained submerged with the sensors in a downward position at a depth of 1–1.5 m. We obtained time series data at a 2 min resolution for turbidity (in Formazin Nephelometric Units, FNU), optical dissolved O_2 (DO, in μmol L^{-1}), and fluorescent dissolved organic matter (*f*DOM; in Quinine Sulphate Units, QSU). Also, the sonde measured the temperature-corrected conductivity (specific conductivity, κ; in μS cm^{-1}) using conductivity electrodes, water temperature (T_w; in °C) using a thermistor, and pH with a glass electrode. The sonde contained a dual-channel fluorescence sensor for determinations of chlorophyll a (chl a), and the accessory pigment for phycocyanin in freshwater blue-green algae (BGA); we report total algae concentrations (TAlgae; in μg L^{-1}) from these measurements (i.e., TAlgae = chl a + BGA). An automatic wiper brush routinely cleaned the optical window of the sensors to prevent fouling interferences due to organic or inorganic deposits during the measurements. The sonde measurements were interrupted between the evenings of 13 July and 14 July 2019 because of a power outage
2. **Acoustic Doppler current meter.** A side-looking acoustic flow meter SonTek-SL1500-3G (Doppler current meter 1,500 kHz; Xylem Inc., San Diego, CA, USA) was mounted on the left side of the channel (facing downstream) at the ARS (Figure 1c). For this, we used a metal and wood mounting system that kept the instrument in a vertical position and submerged it in the water column at a depth of ∼1 m. With falling water levels over time at the river, the instrument was moved to the center of the channel to keep it submerged at the same measuring depth. This instrument was equipped with velocity and water level transducers (pressure sensors) for instantaneous discharge (flow rates) measurements. The water discharge (Q, in m^3 s^{-1}) was calculated with the SonTek-SL Intelligent Flow software (Version 3.0) which is an interface for the SonTek-SL doppler current meter. The cross-sectional shape of the channel was measured on-site at the start of the study. This morphological information, together with the measured water velocity (v), was used to configure the instrument for the calculation of Q. The horizontal reach length of the Doppler beams was 2.7 m (l_m), and the reach angle was not hindered by the EXO2 sonde located at the center of the channel. The flow meter was out of service for eight days (6–14 July 2019) due to technical problems in the installation

Water discharge measurements were sampled every 2 min in parallel with the EXO2 sonde. The data acquired from both instruments were simultaneously stored in a data logger (enviLog Mobil ecoTech®, Bonn, Germany) located at the riverbank of the ARS, where a generator provided continuous electrical power to the system (Figure 1c).

3. **Flow-Through (FT) measurements**. A portable and versatile set-up was installed on the bank of the ARS (Figure 1c) for the continuous monitoring of the partial pressure of carbon dioxide (pCO_2) and methane (pCH_4). For pCO_2, we used a HydroC® CO_2 FT sensor based on non-dispersive infrared absorption spectroscopy. For pCH_4 we used a HydroC® CH_4 FT sensor based on tunable diode laser absorption spectroscopy (-4H-JENA engineering GmbH, Jena, Germany). We measured the temperature and conductivity of the incoming water to the sensors (SBE 45 thermosalinograph sensor; Sea-Bird Electronics, Bellevue, USA), as well as its flow rate with a flowmeter. A submersible pump located 10 m away from the riverbank was secured to a floating buoy with an anchor weight to feed river water continuously from a depth of 1 m to the sensors through PVC tubing submerged to the river bed and insulated on land to reduce variations in in-situ water temperature and exposure to light.

2.3. Discrete Water Sampling for DOC, DOM, and Microbiome Analysis

At the beginning and at the end of the experiment, discrete water samples were collected in four points in the Ambolikha River at a depth of 1 m (Figure 1b; supporting Table S1 in Supporting Information S1). At the ARS (point 1, Figure 1b), the samples were collected next to the EXO2 sonde at the same depth of the sensors. A 1.5 L Niskin bottle was mounted onto a stainless-steel frame to collect water samples for the analysis of DOC (determined through combustion using high-temperature catalytic oxidation) and to characterize the DOM with ultrahigh-resolution mass spectrometry according to established protocols (Koch et al., 2007; Kügler et al., 2019; Leefmann et al., 2019) using a high-resolution-electro spray ionization orbitrap mass spectrometer. We also collected water samples to analyze microbial communities following protocols for DNA isolation, amplicon sequencing, and 16S rRNA gene quantification. In all cases, the respective flask for each analyte was used following standard protocols for natural water analysis, and samples were stored immediately at 4°C for DOM and DOC for no more than 6 hr until preliminary on-site treatment (described in the supporting text S.1.2.). Specific information on the DOM and microbial community analyses is given in the supporting text S.1.3. to S.1.8.

2.4. Water–Gas Flux Calculations

The water-to-air flux densities F (amount area^{-1} time^{-1}) of CO_2, CH_4, and O_2 from the river (FCO_2, FCH_4, and FO_2) were calculated according to:

$$F = k_n \ \Delta C = k_n(C_w - C_{eq}) \quad (1)$$

where the coefficient k_n is the gas transfer velocity (length time^{-1}) calculated with a specific method n (given below) of the respective gas at the in-situ water temperature. C_w is the measured bulk gas concentration in the water and C_{eq} is the calculated water-side equilibrium concentration of that gas; both concentrations are reported in µmol L^{-1}. The calculation of C_{eq} for each gas is described below. The excess gas concentrations are the respective gradients for each gas (g) ($\Delta g = C_w - C_{eq}$).

The measured pCH_4 and pCO_2 were converted to the corresponding C_w using the Bunsen solubility coefficient (β; in mol L^{-1} atm^{-1}) calculated as a function of temperature with the polynomial of Weiss (1970) for pCH_4, and with the polynomial of Weiss (1974) for pCO_2. C_{eq} for O_2 was calculated according to Garcia and Gordon (1992), and for CH_4 was calculated following Wiesenburg and Guinasso (1979). The atmospheric pCO_2 and pCH_4 (in atm) were calculated according to:

$$p = x(P - pH_2O) \quad (2)$$

where x is the dry air mole fraction of CO_2 and CH_4, respectively. P is the barometric pressure and pH_2O is the saturation water vapor pressure at in-situ water temperature (both in atm). We used dry air mole fractions of 409.4 ppm for CO_2 and 1,859 ppb for CH_4, and a standard barometric pressure of 1 atm. The dry mole fractions are

averages of the monthly global values for June and July 2019 from the Global Monitoring Laboratory, NOAA (Dlugokencky, 2019; Dlugokencky & Tans, 2019).

Estimating gas transfer velocities k_n in rivers is highly variable between systems because it depends on numerous factors such as changes in turbulence, geomorphic characteristics of the river channels (e.g., slope), flow velocities, and wind influences (Hall & Ulseth, 2019). Due to large uncertainties in gas transfer velocities in flowing systems obtained from different methods, we compared the results of k_n calculated using four different approaches: 1) with the empirical parametrization of Wanninkhof (2014) using the wind speed at 10 m above the water surface (u_{10}, m s^{-1}): $k\_W14 = 0.251u_{10}^2$. We calculated u_{10} following Amorocho and Devries (1980) and using the wind speed u from the eddy tower measured ~8 m above the surface of the Ambolikha River (taking into account the height of the anemometer at 5 m above ground and the average height of 3 m from the surface water to the plateau of the riverbank). 2) The open-channel method for night-time drop in oxygen concentration (Odum, 1956), referred to here as k_O56, calculated with the RIVERMET© program (Izagirre et al., 2007). This method relies on the diel changes of DO concentration attributed to photosynthetic O_2 production during the day, and constant respiration (or O_2 consumption) during the night. 3) Using a typical approach for lotic systems with a hydraulic model based on measurements of stream velocity (V, m s^{-1}) and the mean channel slope (S, unitless) (Raymond et al., 2012): $k\_R12 = 2841(V \times S) + 2.02$, and supporting text S.1.9. 4). 4) With a wind parameterization for a freshwater lake based on inert trace-gas addition (Cole & Caraco, 1998): $k\_CC98 = 2.07 + 0.215u_{10}^{1.7}$. The k_W14, k_O56, k_R12 and k_CC98 values are standardized with the corresponding Schmidt number (Sc) as a function of water temperature for each gas with reference to Sc for CO_2 (i.e., 600) at 20°C in freshwaters (Wanninkhof, 1992), with n being either W14, O56, R12 or CC98.

$$k_n = k\_n \times \left(\frac{Sc}{600}\right)^{-0.5} \quad (3)$$

2.5. Land Gas Fluxes and Meteorological Data

The land gas fluxes and meteorological parameters were measured with an eddy covariance (EC) tower located at ~500 m to the northwest of the ARS (68° 37' 0.82" N, 161° 21' 2.37" E) in a wet tussock tundra area at the floodplain (Göckede et al., 2017; Kittler et al., 2017) (Figure 1b). The EC instrument was equipped with a heated sonic anemometer (uSonic-3 Scientific, 5 W heating, Metek GmbH, Elmshorn, Germany) and a closed-path gas analyzer (FGGA, Los Gatos Research Inc., CA, USA) used to monitor the CO_2, H_2O, and CH_4 mixing ratios at the height of 5 m above the land surface. The EC data were collected at a frequency of 20 Hz. With these measurements, we obtained the land net ecosystem exchange (NEE) and the terrestrial flux of CH_4 (FCH_{4_land}) at 30 min resolution. The NEE represents the net flux of CO_2 mostly between the vegetation, soil, and the atmosphere within the footprint of the eddy tower with an estimated area of 0.8 km^2 that is generally not influenced by the riverine gas emissions. A negative NEE value indicates a net uptake of CO_2 by the vegetation. The meteorological data were measured every 10 s (wind speed and direction, short- and long-wave downward and upward radiation, relative humidity, pressure, and air temperature at 6 m above ground), and averaged every 30 min during data post-processing. Detailed information on the set-up, data collection, and EC data post-processing for the quality control and the flagging system are described in detail in Kittler et al. (2016) and Kittler et al. (2017).

2.6. Comparison Between Land and Water Gas Fluxes

The CO_2 and CH_4 flux densities over land and water are expressed in mol $area^{-1}$ $time^{-1}$. To obtain the riverine emissions following Equation 1, we used the k_{R12} values. The land and water fluxes were converted to gC $area^{-1}$ $time^{-1}$ in terms of the amount of carbon in CO_2 (C-CO_2), or in CH_4 (C-CH_4), using the molar weight of carbon accordingly. The FO_2 was calculated in terms of C (i.e., FCO_{2RQ}) using a generalized respiratory quotient (RQ) of 1.35 for net heterotrophic freshwater systems (Berggren et al., 2012). Thus, considering that the consumption of a mole of O_2 produces 1.35 moles of CO_2, we multiplied FO_2 (mol O_2 $area^{-1}$ $time^{-1}$) times −1.35 to obtain FCO_{2RQ}. We assumed that the calculated CO_2 remained in this form within the aquatic system during our measurements (i.e., CO_2 does not suffer further transformation to carbonates). FCO_{2RQ} was then converted to gC $area^{-1}$ $time^{-1}$ to obtain surface emission rates. The cumulative fluxes for the 38 days of the study (gC m^{-2}) were used to compare the land and water carbon fluxes.

2.7. Water Residence Time in the Ambolikha River

We defined the integrated residence time (iT_R) of a water parcel in the river as the average time that it takes to travel through a defined channel segment (Jones et al., 2017). We calculated iT_R using the cumulative sum of the water discharged through a fixed segment length (l) in the river channel of 10 km, which is the distance between point 1 (at the ARS) as upstream limit, and point 3 as downstream limit which is a point where the main channel retains a similar width (Figure 1b). Because this approach does not consider variations in the width and depth in different water paths (e.g., the deepest water path or thalweg) along the channel length, the water velocity is assumed to be homogeneous across the channel cross-section. We also assumed the same temporal variation in water depth at the selected channel segment, taking as reference the changes in water depth at the ARS. At the start of the study, we measured the depth profile at a cross section of the river channel at the ARS and found a typical trapezoidal shape with a flat river bed and an open channel of 50 m in width (w).

2.8. Data Quality Control and Calibration

We obtained five groups of time series that represent the measurements taken during this study at the ARS: (a) water properties at mooring location, (b) water flow meter data (both with 2 min temporal resolution), (c) water pCO_2 and pCH_4 (5 s temporal resolution); and, at the Ambolikha floodplain: (d) land fluxes, and (e) meteorological data (both with 30 min temporal resolution). Each data set was individually assessed for quality control purposes, including potential errors in the measurements, power outages, or water pump malfunctions. The flow meter data was checked for errors due to interferences to the Doppler beam reach, wrong angle of the instrument, or power outages.

2.8.1. Calibration of EXO2 Sonde Sensors

All sensors were factory calibrated prior to fieldwork. Sensor-specific two-point calibrations for DO and pH were performed on-site before deployment following the manufacturer's manual. No large analytical drift was observed in the sensors' readings before and after the deployment. On-site sensor recalibration additionally supported this after the measurement period. The effect of temperature on the measured chl a and BGA determinations was considered during the factory calibration procedure through the use of a calibration standard. The total algae biomass (TAlgae), is an estimate of pigment concentration obtained from the correlation between the measured relative fluorescent units and pigment extracted under laboratory conditions during the factory calibration. As we did not independently compare the concentration of these pigments with other established spectrophotometric methods from live samples from our study site, we use the TAlgae measurements as an uncorrected reference of the algal presence in our site. The fluorescent dissolved organic matter (fDOM) measurements represent the abundance of the humic substances contained in the dissolved organic matter at the mooring site, which have fluorescent properties when they are exposed to a near-ultraviolet light (wavelength of excitation of 365 ± 5 nm and fluorescent emissions of 480 ± 40 nm). The measured fDOM data was corrected due to sensor response to temperature effects for a reference temperature of 25°C (Downing et al., 2012; Watras et al., 2011). The temperature-corrected fDOM was further corrected due to sensor response to light attenuation influenced by turbidity as measured with the EXO2 sonde following Snyder et al. (2018).

2.8.2. Calibration of Flow-Through Sensors and Data Corrections

The HydroC® CO_2 FT and CH_4 FT sensors were individually factory-calibrated before and after the deployment. For calibration of the CO_2 sensor, regular interval 'zeroings' were automatically conducted approximately every 5 hr during the deployment, allowing for a linear zero drift correction. The slope drift correction for CO_2 was applied after the deployment by correcting the slope linearly over sensor runtime between the pre- and post-deployment polynomials. For CH_4, there was no need for drift corrections because the derivative signal is directly proportional to CH_4. Compared to CO_2, CH_4 is less soluble in water, less permeable to the membrane material in the sensor and it is required a larger internal gas volume during the measurements, thus the response time (RT) of CH_4 to the sensor tends to be longer. However, an RT correction was not applied in our data due to sufficient exposure time of the water to the sensor and smooth changes between concentrations gradients over time. Further corrections of the pCO_2 and pCH_4 due to the water temperature variations were applied and details are given in the supporting text S.1.10. For more in-depth data corrections see Canning et al. (2021) and Fietzek et al. (2014). Periods of missing data are related to issues with the submerged pump, failure in internal values, and insufficient flow rates.

2.8.3. Statistical Analysis

After calibration and quality control assessments, all the time series were harmonized to 30 min using centered moving averages from the 2 min and 5 s data sets correspondingly. Timestamps were matched to the nearest time, using the eddy covariance and meteorological data as a reference. We tested independently the presence of the first-order temporal autocorrelation, ACR(1), in selected time series datasets before further statistical analysis. For this, we used a Durbin-Watson statistical test (Hilbe, 2014). If ACR(1) was detected, we applied a Cochrane-Orcutt procedure (Cochrane & Orcutt, 1949; Wooldridge, 2013) using iterative ordinary least squares regressions to reduce the error in the residuals and eliminate the autocorrelation. The resulting non-autocorrelated time series were correlated with each other by using a pair-wise Pearson linear correlation analysis ($p < 0.05$) to find possible dependencies between the measured variables. All raw data of the selected 30-min time series contained ACR(1) to some degree. The r^2 values resulting from the correlation analysis between autocorrelated time series were inflated by an average of 18 ± 24 than with the non-autocorrelated time series. For analysis of diel cycles, we first statistically detrended each raw 30-min time series (fitted linear trend) to remove the influences that are longer than a daily cycle in the time series, and extracted the diel cycle per 24-hr cycle to obtain a total of 38 diel cycles for each parameter. Furthermore, we also extracted the diel cycles in the non-autocorrelated time series computed as above, to be able to perform a pair-wise Pearson linear correlation analysis ($p < 0.05$) between the 38-day mean diel cycles of each parameter and find dependencies between them. A negligible difference between the r^2 values (0.02 ± 0.20) was obtained after comparing the results of the correlations between diel cycles from the raw and from the non-autocorrelated signals.

To define the day- and night-time periods in a diel cycle, we followed the 38 days average of the diel cycle in the incoming net solar radiation (i.e., the sum of short- and long-wave downward radiations) measured in the meteorological station. The maximum radiation peak was reached in the afternoon (ca. 14:00 hr local Chersky time) whereas the minima occurred at midnight. Hence, we defined daytime as the period between 08:00 hr and 19:30 hr, and nighttime between 20:00 hr and 07:30 hr local Chersky time.

The peak-to-peak amplitude of the diel cycle was calculated as the difference between the minimum and maximum values for the average diel cycle, with a sign convention for positive values as an average increase of the parameter during the day (i.e., daytime maximum), and negative values as a daytime decrease (i.e., nighttime maximum). The statistical analysis of the data and plots were done using Matlab® (The MathWorks, Inc., MA).

3. Results

3.1. Water Flow Regime and Its Role in Water Properties Measured at the Ambolikha River Site (ARS)

The water discharge (Q) measured at the ARS (Figure 1) portrayed a decrease from the late freshet to summer (Figure 2a), which is in agreement with the decreasing phase of the peak freshet discharge in the Kolyma River (Figure S1 in Supporting Information S1) (Shiklomanov et al., 2020). Notably, in our study, the temporal changes in the magnitude and direction of the water discharge influenced the water properties and biogeochemistry at the ARS. To analyze these changes, the time series was divided into three phases: **Phase 1** covering the initial 19 days (from 26 June 2019 at 15:30 hr to 14 July 2019 at 17:59 hr, local Chersky time), **Phase 2** covering 7 days (from 14 July 2019 at 18:00 hr to 21 July 2019 at 20:59 hr), and **Phase 3** covering the last 12 days (from 21 July 2019 at 21:00 hr to 2 August 2019 at 23:30 hr), that were defined based on the variations in water flow (Figure 2a). The highest Q value (28.9 $m^3\ s^{-1}$) measured in the study was at the late freshet in **Phase 1**. During this phase, the downstream flow (positive Q values) heading toward the main stem of the Kolyma River decreased steadily over time, while the specific conductivity (κ), pH, and turbidity increased (Figures 2a–2c). The calculated water retention time (iT_R) indicated that at the start of **Phase 1** (between 28 June 2019 and 2 July 2019) the average time it took for a water parcel to travel downstream from the ARS to point 3 (channel section that was 10-km long; Figure 1b) was about 1 day. However, the retention time increased gradually from 2 July 2019 onwards, and this was driven by the recurrent change in the flow direction (Figure 2a). In the evening of 16 July 2019 (during **Phase 2**), the direction of Q changed from downstream to upstream and toward the inland direction (negative Q values) and resumed to downstream flow after two days. The measured water properties at the ARS responded to the 2-day water flow inversion, resulting in colder water (T_w, decreased by 1.9°C), higher κ (98.9 µS cm^{-1}), higher turbidity (8.8 FNU), and an increase in the dissolved oxygen (DO) concentration (37.5 µmol L^{-1}).

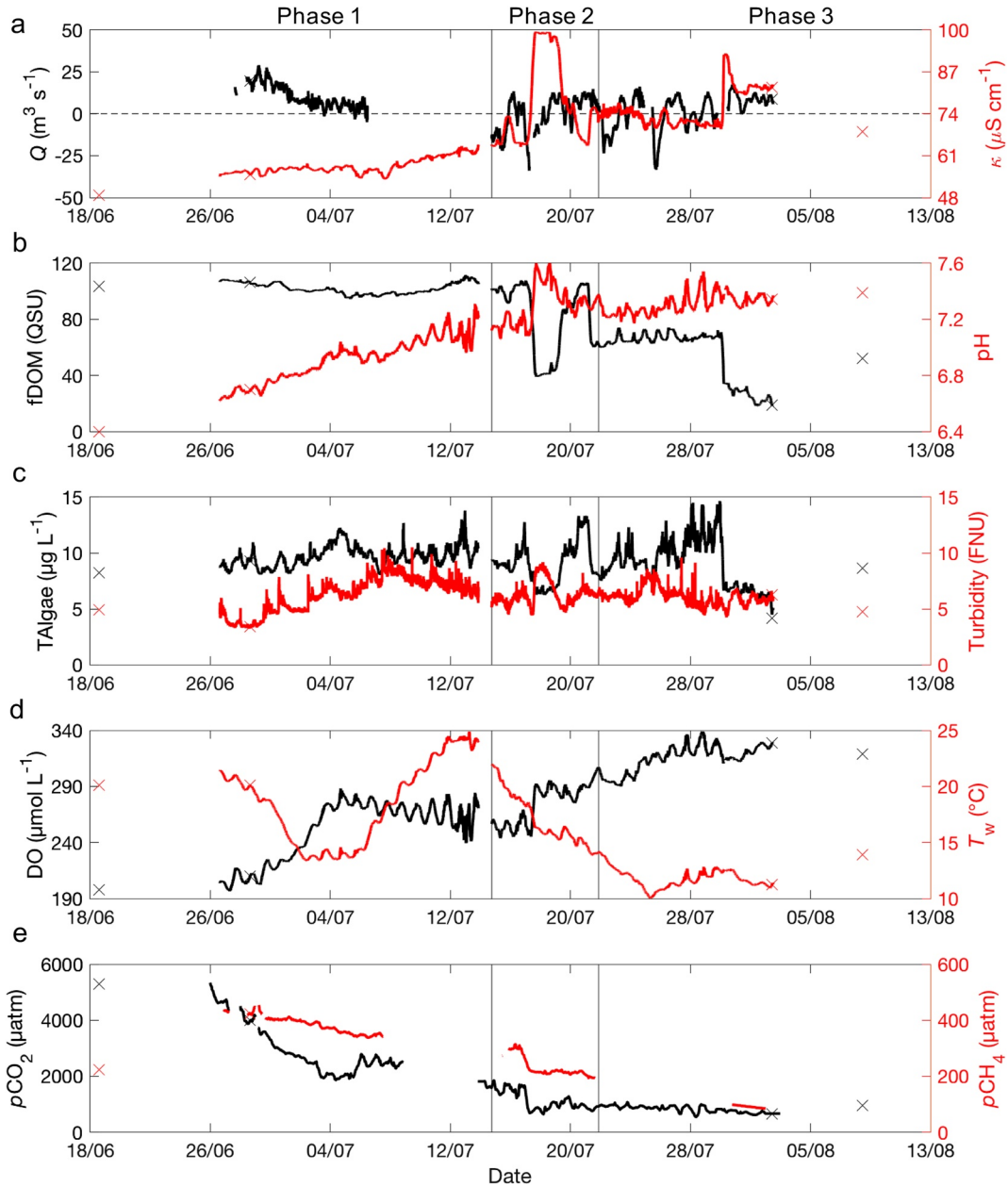

Figure 2. Time series of water properties measured at the Ambolikha River Site. Panels (a), (b), (d), and (e) are data at 2-min resolution, (c) TAlgae at 30-min resolution. Measurement period: 26 June to 02 August 2019. Defined three phases: Phase 1, from 26 June 15:30 hr to 14 July 17:59 hr; Phase 2, from 14 July 18:00 hr to 21 July 20:59 hr, and Phase 3, from 21 July 21:00 hr to 2 August 23:30 hr. The corresponding value for each parameter associated to the discrete samples (where applicable) collected outside the period of the time series are shown with black and red crosses, that is, in dd/mm format: 18/06, 28/06, 02/08, and 08/08, in 2019.

*f*DOM, TAlgae, and pH were also influenced during this period (Figures 2b and 2c), and pCO_2 and pCH_4 decreased by 986 µatm (40%) and 79 µatm (73%), respectively, compared to the values at the beginning of the inversion (Figure 2e). Independent of the flow inversion, by the end of **Phase 2**, the value of T_w decreased by 10.8°C, DO increased to 306.2 µmol L^{-1}, and pCO_2 and pCH_4 decreased further to 807 and 193 µatm, respectively (Figure 2). From 21 July 2019, **Phase 3** was characterized by more frequent changes in the magnitude and direction of Q. In contrast to **Phase 1**, the cumulative volume of the discharges during **Phases 2** and **3** within the 10-km channel segment did not equal the total volume of the segment. Thus, from the evening of 14 July 2019 until at least the completion of our measurements, the water parcel traveling downstream or upstream remained within

the section delimited by points 1 and 3. The variability of Q influenced the water depth at the ARS, with a notable change observed between 2 and 3.5 m during the study period (average ± 1σ. deviation of 2.6 ± 0.45 m; $n = 9$).

The pCO_2 and pCH_4 concentrations at the ARS remained strongly supersaturated with respect to atmospheric equilibrium, and decreased steadily until the end of the study period. The pCO_2 and pCH_4 values were 10 and 5 times greater during **Phase 1** than at the end of **Phase 3**, respectively (Figure 2e; maximum and minimum values in Table 1). The excess gas concentrations (Δg), decreased from the start of **Phase 1** until the end of **Phase 3** by about 90% for CO_2 (Table 1). This represented a decrease in supersaturation from 1083% to 64%. Similarly, the excess concentration of CH_4 decreased by 78%, with supersaturation levels declining from 23,422% (or of the order of 200 times at equilibrium with the atmosphere) at the beginning of the study, to 4343% at the end. During **Phase 1**, we measured the lowest DO at 30% (undersaturation) with respect to the atmospheric equilibrium, with the second-highest T_w (21.5°C). Throughout the study, the DO concentration was predominantly undersaturated, with an average deficit of O_2 of 11 ± 8% (or −34.4 ± 25 μmol L^{-1}). However, the DO increased from 203 μmol L^{-1} to 302 μmol L^{-1} (i.e., a 50% increase from the initial concentration) from the beginning to the end of the study period, representing a decrease in the undersaturation levels from 26% at the beginning to 4% at the end of the study period. Only sporadic nighttime DO supersaturations where measured between 11–13 July 2019, which resulted in an O_2 excess of up to 18.7 μmol L^{-1} (7% supersaturation).

3.2. Gas Fluxes From the River and Floodplain

The resulting k_n values calculated from the four methods explained in Section 2 indicate large variations. Consequently, the magnitudes of the riverine gas emissions have large uncertainties because they are determined by the value of k_n. In our study, the mean k_n value calculated using the marine-wind speed parameterization ($k_{W14} = 0.9 \pm 0.6$ m d^{-1}) is in good agreement with the average k_n value calculated using the lake-wind parameterization ($k_{CC98} = 0.9 \pm 0.4$ m d^{-1}). These values were half the average k_n value calculated using the nighttime oxygen drop method ($k_{O56} = 2.2 \pm 1.3$ m d^{-1}) and the mean k_n value calculated using the hydraulic channel properties ($k_{R12} = 1.9 \pm 0.2$ m d^{-1}). Similarly, the mean gas fluxes of CO_2, CH_4, and O_2 calculated with k_{W14} ($FCO_2 = 0.5 \pm 0.6$; $FCH_4 = 0.004 \pm 0.003$; and $FO_2 = -0.4 \pm 0.4$, all in μmol m^{-2} s^{-1}), were in the same range of values calculated with k_{CC98} ($FCO_2 = 0.6 \pm 0.5$; $FCH_4 = 0.005 \pm 0.002$; and $FO_2 = -0.4 \pm 0.3$, all in μmol m^{-2} s^{-1}). These values are nearly half the flux values calculated with k_{O56} ($FCO_2 = 1.3 \pm 0.9$; $FCH_4 = 0.010 \pm 0.005$; and $FO_2 = -0.9 \pm 0.7$, all in μmol m^{-2} s^{-1}) (Table 1).

The Ambolikha River is a floodplain channel that behaves both as a lotic and lentic ecosystem, thus, hydraulic models for rivers might not capture the processes that generate water turbulence and the variations in flow direction over time. Additionally, k_n from lake-wind or marine-wind parameterizations capture only a partial picture of these systems because they rely only on the wind speed. The average k_{R12} value calculated in our study was closer to other gas transfer velocities previously reported in Arctic rivers and streams (Table 2); thus, in our study, we chose the riverine fluxes calculated using k_{R12} values for further discussion and comparison between water and land gas emissions.

The time-series data of the water gas fluxes revealed a symmetrical pattern indicating that larger outgassing of FCO_2 and FCH_4 occurred during larger uptake of FO_2 and vice versa, consistent with the observed anticorrelation between the excess gas concentrations (Figure 3). The gas flux estimate contains large uncertainties that are inherent to the method selected for the calculation of k_n. We provide an estimate of the uncertainty of the flux values for each gas, using the standard deviation (±1σ) of the ensemble mean obtained with the results of the four k_n models tested in this study (shaded area around the flux calculated with k_{R12} in Figures 3a and 3b). The flux of gases calculated with k_{R12} falls in the upper end of the uncertainty range, but according to our estimates, they can be up to two orders of magnitude smaller considering other k_n models that are based on wind speed (i.e., W14 and CC98). The uncertainty in the fluxes is larger as the concentration of dissolved gases is also higher (i.e., during late freshet), and the difference between the values of the fluxes calculated with different methods becomes smaller, as the gases approach equilibrium conditions (i.e., during summer) (Figures 3a and 3b).

The linear correlation analysis between the calculated fluxes resulted in a negative linear correlation with $r^2 = 0.03$ (statistically significant at $p < 0.05$) between the time series of FO_2 and FCH_4; whereas no significant correlation was obtained between these fluxes and FCO_2. In contrast to the aquatic FCO_2, the time series data from the net ecosystem exchange (NEE) in the floodplain indicated dominant CO_2 uptake during the study period, with an

Table 1
Summary of Average, Minimum and Maximum Values, and 38-Day Average Values of the Amplitude of the Diel Cycles of Selected Parameters Measured in Water and Atmosphere in Ambolikha Site From 26 June 2019 to 2 August 2019 From the 30 min Averaged Time Series (Raw).

Parameter	Symbol (units)	Mean ± 1 std.	Min.	Max.	Daily mean ± 1 std. diel cycle amplitude
Water					
Water velocity	V (m s^{-1})	0.03 ± 0.08	−0.24	0.21	(−) 0.11 ± 0.06
Water discharge	Q (m^3 s^{-1})	4.1 ± 10.0	−32.1	27.9	(−) 14.4 ± 8.1
Depth	z (m)	2.7 ± 0.45	2.2	3.5	–
Water temperature	T_w (°C)	15.9 ± 4.0	10.1	24.8	(+) 1.1 ± 0.7
Specific conductivity	κ (µS cm^{-1})	67.4 ± 11.4	53.8	99.2	(+) 4.9 ± 7.3
Salinity	S	0.04 ± 0.007	0.03	0.059	(+) 0.003 ± 0.004
pH	pH	7.1 ± 0.2	6.6	7.6	(+) 0.12 ± 0.08
Turbidity	Turbidity (FNU)	6.2 ± 1.2	3.3	9.5	(+) 1.4 ± 0.8
Total algae	TAlgae (µg L^{-1})	9.3 ± 1.6	4.3	14.0	(+) 2.4 ± 1.5
	chl a (µg L^{-1})	8.7 ± 1.4	–	–	–
Fluorescent dissolved organic matter	*f*DOM (QSU)	81.9 ± 26.5	18.4	110.7	(−) 10.1 ± 15.1
Partial pressure of CO_2	pCO_2 (µatm)	1689 ± 1108	536	5344	(−) 342 ± 222
Partial pressure of CH_4	pCH_4 (µatm)	292 ± 109	84	454	(−) 18 ± 15
Dissolved oxygen	DO (µmol L^{-1})	276.9 ± 35.5	197.4	338.1	(+) 15.6 ± 9.4
	(mg L^{-1})	8.9 ± 1.1	6.3	10.8	(+) 0.5 ± 0.3
Excess CO_2	ΔCO_2 (µmol L^{-1})	54 ± 41	13	167	(−) 13.8 ± 8.7
Excess CH_4	ΔCH_4 (µmol L^{-1})	0.46 ± 0.17	0.15	0.67	(−) 0.03 ± 0.02
Excess O_2	ΔO_2 (µmol L^{-1})	−34 ± 25	−89.7	18.7	(+) 19.4 ± 8.4

Parameter	Symbol (units)	Mean ± 1 std.	Min.	Max.	38-day mean ± 1 std. diel cycle amplitude
River					
Gas transfer velocity*	k_n(m d^{-1})	1.9 ± 0.2	1.5	2.8	–
Flux of CO_2* Cumulative	FCO_2 (µmol m^{-2} s^{-1}) (gC-CO_2 m^{-2})	1.1 ± 0.9 36.8^	0.1	4.1	(+) 0.4 ± 0.2
Flux of CH_4* Cumulative	FCH_4 (µmol m^{-2} s^{-1}) (gC-CH_4 m^{-2})	0.01 ± 0.004 0.21^	0.003	0.02	(+) 0.01 ± 0.0008
Flux of O_2* Cumulative (RQ = 1.35)	FO_2 (µmol m^{-2} s^{-1}) (gC-O_2 m^{-2})	−0.9 ± 0.6 60.6^	−2.8	0.6	(+) 0.4 ± 0.2
Land					
Net Ecosystem Exchange Cumulative	NEE (µmol m^{-2} s^{-1} (gC-CO2 m^{-2})	−3.4 ± 4.1 −168.9^	−14.6	4.9	(−) 12.5 ± 3.1
Ecosystem Respiration Cumulative	ER (µmol m^{-2} s^{-1}) (gC-CO2 m^{-2})	2.1 ± 0.5 103.0^	1.3	4.9	–
Flux of CH_4 in floodplain Cumulative	FCH4_land (µmol m^{-2} s^{-1}) (gC-CH4 m^{-2})	0.07 ± 0.02 3.3^	−0.04	0.3	(+) (9 ± 6) ×10^{-2}
Atmosphere					
Air Temperature (6 m above ground)	T_a (°C)	11.5 ± 6.8	1.8	31.3	(+) 7.8 ± 3.4
Wind speed (10 m above water surface)	u_{10} (m s^{-1})	3.6 ± 1.6	0.3	8.2	(+) 4.2 ± 1.3

*k_n Value and Fluxes Calculated Using Raymond et al., (2012); ^Total Cumulative Flux; RQ = Respiratory Quotient.

Notes. The sign between parenthesis in the values of last column indicates the presence of an average daytime maximum (positive), or an average nighttime maximum (negative) in the diel cycle.

Journal of Geophysical Research: Biogeosciences

10.1029/2021JG006485

Table 2
Summary of Comparison to Other Studies, for pCO_2 and pCH_4 and Their Fluxes From Other Arctic Rivers and Streams

Site	pCO_2 (µatm)	ΔCO_2 (µmol L^{-1})	FCO_2* (µmol m^{-2} s^{-1})	pCH_4 (µatm)	ΔCH_4 (µmol L^{-1})	FCH_4[a] (µmol m^{-2} s^{-1})	k_n (m d^{-1})	Reference
Kuparuk River, Alaska	812 ± 177	–	0.13 ± 0.02	236	–	0.004	0.5[b]	Kling et al. (1991)
Yukon River, North America	>1,500	100	2.4–6.3	8.4 (main stem)	0.2 (main stem); 0.6 (tributaries)	0.03 (tributaries)	5.2	Striegl et al. (2012)
Rivers and streams in Northern Quebec	2959	–	–	1781	–	–	1.12	Campeau & del Giorgio (2014)
Pristine streams in NWT, Canada	1,085 (529–3,186)	–	1.92 (0.5–5.8)	33.1 (0.04–318.9)	–	0.007 (−0.02–0.09)	6.6 (CO_2); 0.9 (CH_4)	Zolkos et al., 2019
Kuparuk River	925 ± 3 ppm	–	3.73 ± 0.64	–	–	–	7.6	Rocher-Ros et al. (2020) [c]
Toolik River	1878 ± 16 ppm	–	2.15 ± 1.4	–	–	–	2.2	
Tributaries of Lena River	400–1600	–	0.13–5.2	–	–	–	4.46	Vorobyev et al. (2021)
Ambolikha River (Tributary of Kolyma River)	707	–	0.72	–	–	–	3.9 ± 2.5	Denfeld et al. (2013)
	1689 ± 1108	**54**	**1.1 ± 0.9**	**292 ± 109**	**0.46**	**0.01 ± 0.004**	**0.9 ± 0.7 (W14)** **0.9 ± 0.4 (CC98)** **1.9 ± 0.2 (R12)** **2.2 ± 1.3 (O56)**	**This study**

[a]Fluxes calculated using k_n from Raymond et al., (2012) (k_{R12}). [b]Calculated with wind lake models, but can be too small for this river and the CO_2 fluxes may be underestimated (Kling et al., 1991). [c]The k_n values provided in Rocher-Ros et al. (2020) were obtained with a reaeration model that was previously used for lakes, thus the fluxes can be overestimated.

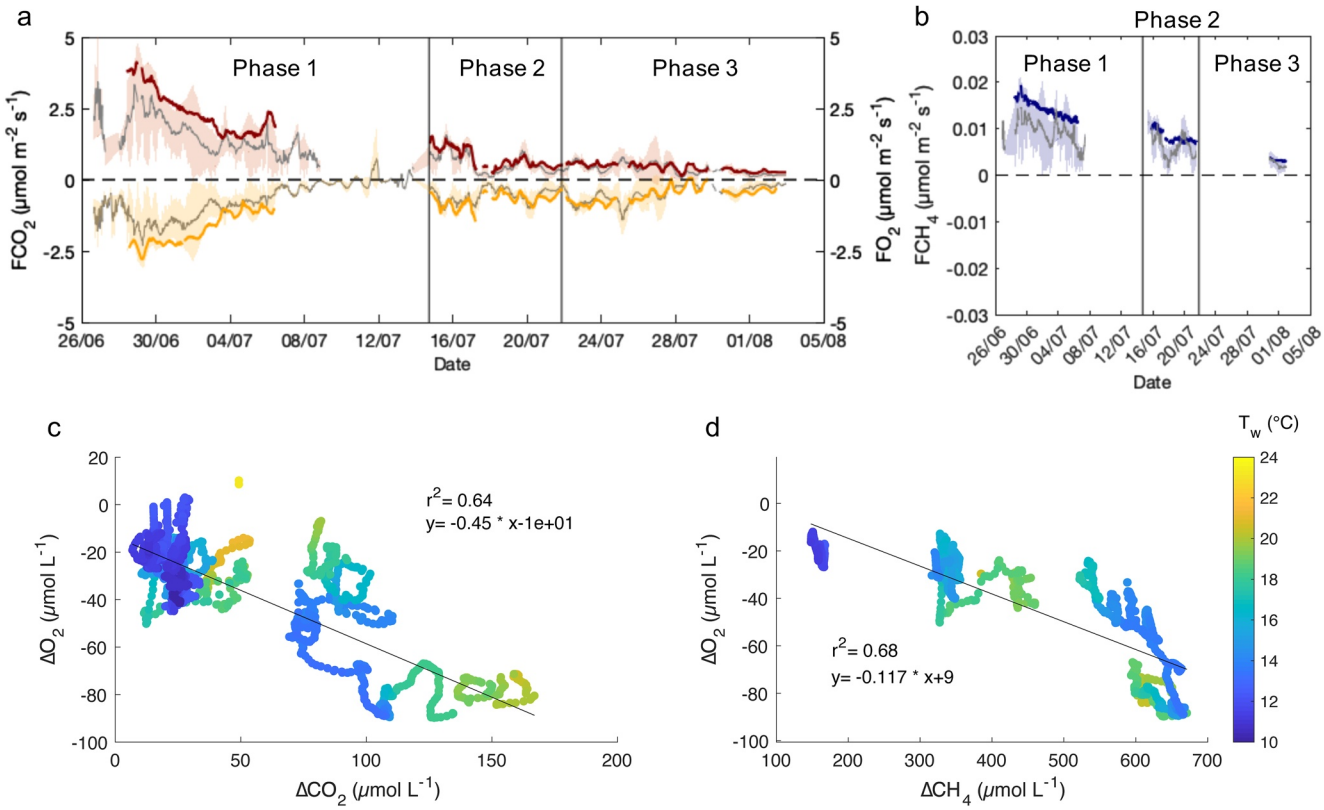

Figure 3. Time series of the flux of CO_2, CH_4, and O_2. (a) and (b) show the times series of water gas fluxes calculated with k_{R12}, with positive values as emissions to the atmosphere and negative values as uptake. The average of the ensemble of fluxes calculated with four k_n models for each gas is shown (gray line) surrounded by colored shaded areas depicting the uncertainty ($\pm 1\sigma$) of the ensemble mean. (c) and (d) show the linear correlation analysis between the excess of the water flux of gases using the original time series.

average value of -3.4 ± 4.1 µmol m^{-2} s^{-1} (Figure 4a). The flux of methane from the floodplain (FCH_{4_land}) was always positive, with emissions to the atmosphere averaging at $(7 \pm 2) \times 10^{-2}$ µmol m^{-2} s^{-1} during the study period (Figure 4b). The time series of T_w and air temperature (T_a) indicated a positive correlation ($r^2 = 0.01$), reflected by similar variations over time, although T_w had a delayed response of 2–3 days compared to T_a (Figure 4c).

3.3. Identification of Diel Cycles and Correlations

Owing to the high temporal resolution of our continuous measurements, we found evidence for daily diel cycles in nearly all the measured parameters, despite the muted diel variability in incoming radiation during the Arctic summer (Figure 5). The diel cycle of the net radiation (Figure 5a) seemed to have influenced T_w and T_a ($r^2 = 0.15$ and 0.83 respectively, at $p < 0.05$; using the diel cycles consistently from the non-autocorrelated time series). The mean diel cycles of T_w and T_a ($r^2 = 0.12$) reached a minimum (T_w of 15.7°C and T_a of 8.5°C) before noon and a maximum (T_w of 16.4°C and T_a of 14.3°C) during the day, with a larger average daily change in T_a (5.7°C) compared to T_w (1.1°C) (Figure 5b). During an average day, T_a reached its minimum six hours earlier than the daily minimum of T_w; the maximum values were achieved about three hours earlier for T_a, in agreement with the temporal shift observed in the time series (Figure 4c). The daytime increase of T_w seemed to have influenced the daily variation of some of the measured aquatic parameters. T_w correlated positively with pH and DO ($r^2 = 0.36$) and pCO_2 ($r^2 = 0.22$) Figures 5b–5e). DO and pCO_2 also increased during the day ($r^2 = 0.32$), along with TAlgae ($r^2 = 0.22$ against DO, and 0.14 against pCO_2) (Figure 5c). The daytime increase in pCO_2 (and pCH_4) was moderate in comparison to the steeper shift observed between the night maximum and the midday minimum (Figure 5d).

The correlation between Q and fDOM was not statistically significant, despite the fact that during the night time, both parameters achieved the daily maxima (Figures 5e and 5f). In contrast, the diel cycles of fDOM and κ were

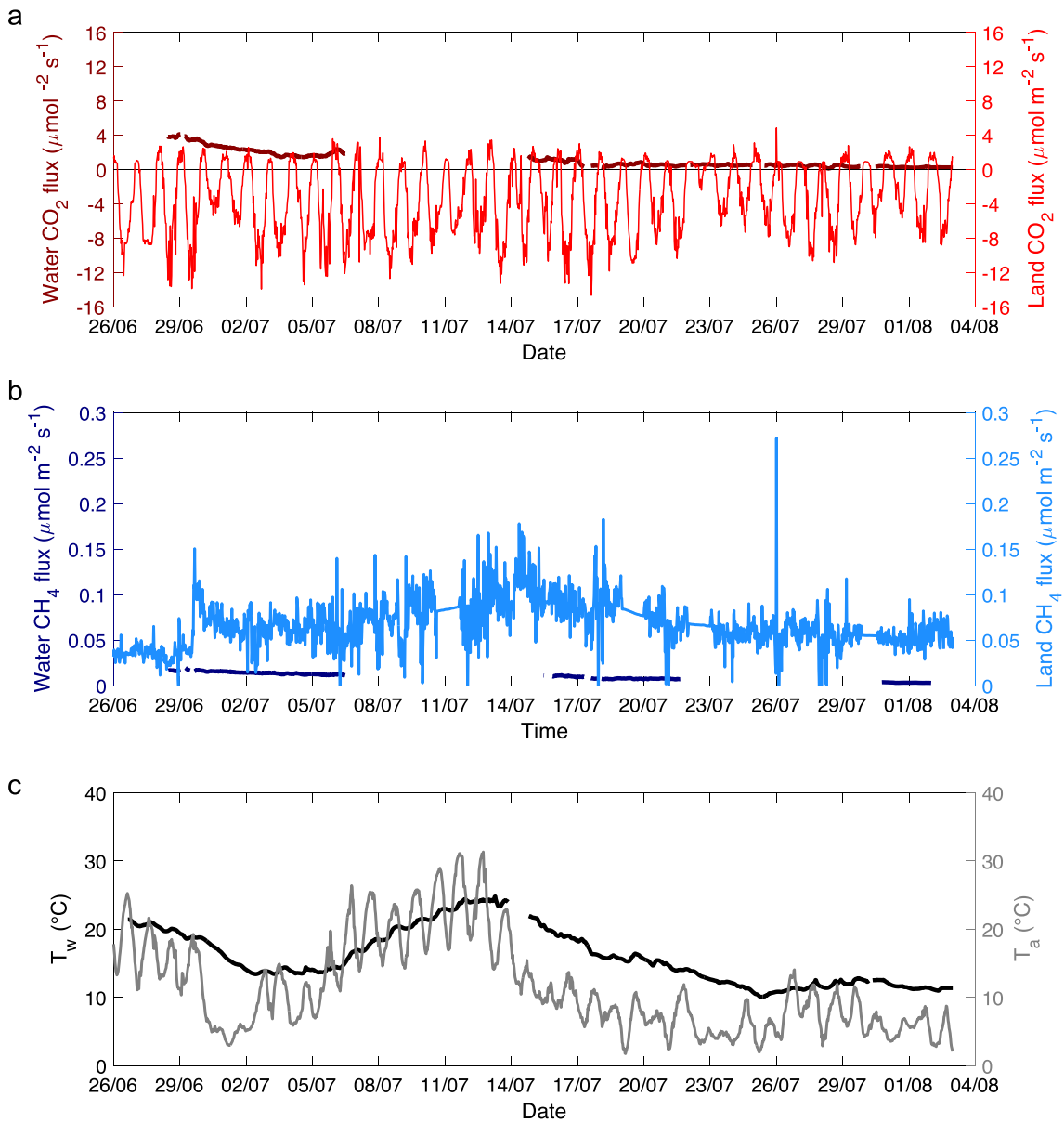

Figure 4. Time series of water and land parameters measured at the Ambolikha River site and floodplain, (a) CO_2 fluxes, (b) CH_4 fluxes and (c) water and air temperatures (T_w and T_a).

negatively correlated ($r^2 = 0.09$), indicating an abundance of organic optical fluorescent substances when less conductive substances were present at the ARS. The diel cycle of turbidity indicated an average increase during the day, but only a statistically significant negative correlation was observed when turbidity was correlated to pCH_4 ($r^2 = 0.01$). Contrarily, turbidity seemed to have a major influence during larger time scales (i.e., more than one day) compared to other parameters. Positive correlations were observed for time series scale between turbidity and Q, κ, DO, and fDOM ($0.01 < r^2 < 0.02$).

In the diel cycles of the aquatic gas fluxes (Figures 5g–5i), FCO_2 increased during the day, whereas FCH_4 shows a less clear trend; hence the correlation between FCO_2 and FCH_4 was not statistically significant. The FO_2 average diel cycle followed the same pattern as DO (Figures 5g and 5c), with the daytime build up reflecting a weakened O_2 sink (i.e., less negative FO_2) between 8:00 hr and 17:00 hr. The FO_2 average diel cycle correlated positively to the average diel cycle of FCO_2 ($r^2 = 0.18$). The correlation between the average diel cycles of FO_2 and FCH_4 was not statistically significant, contrary to the correlation between the times series of both fluxes ($r^2 = 0.03$).

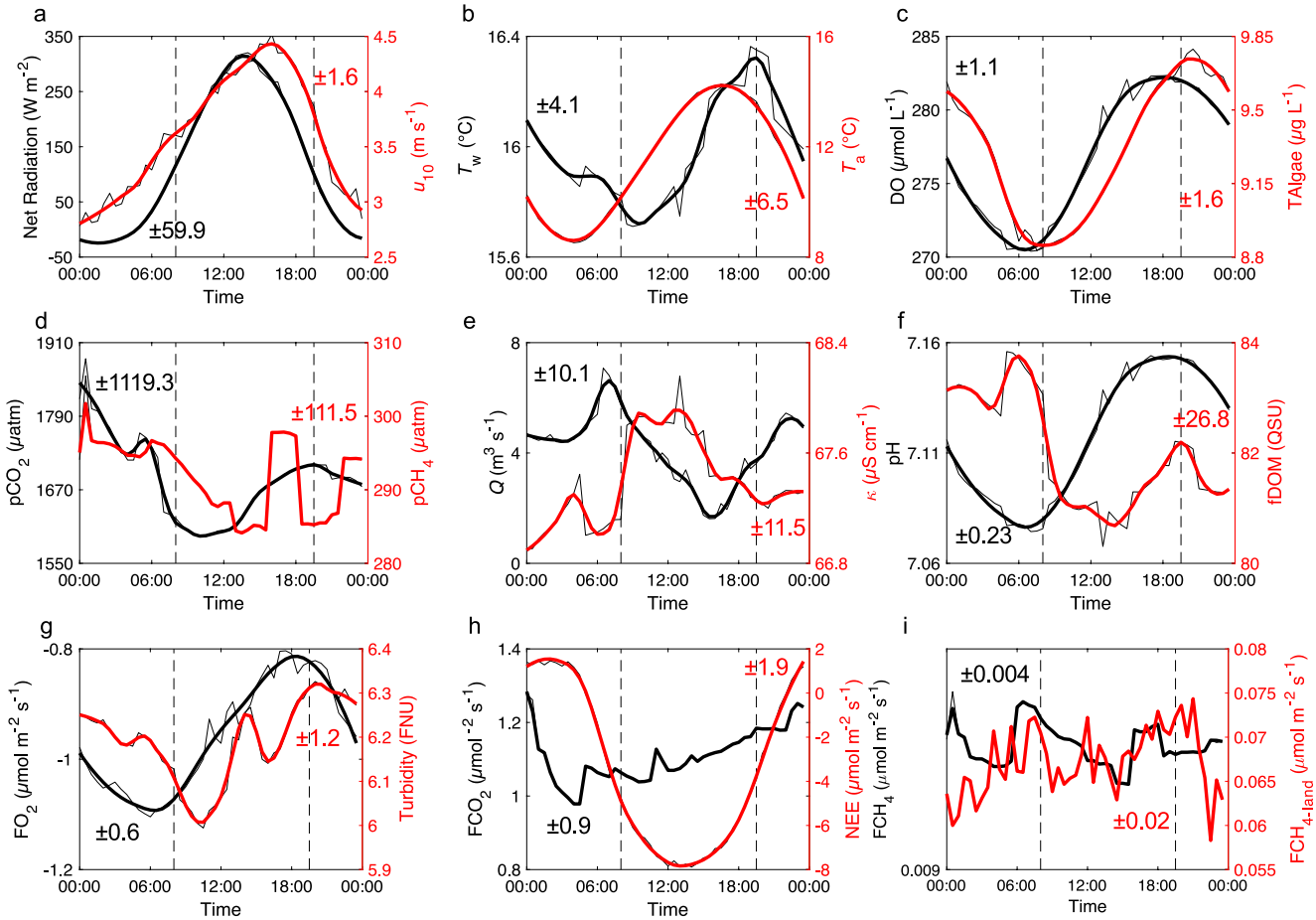

Figure 5. Diel cycles of water and atmospheric parameters. 38-day mean of the diel cycles (black thin line) and centered moving averages (bold black and red lines) calculated from the original time series). Daytime (08:00 hr to 19:30 hr) and nighttime (20:00 hr to 07:30 hr) are delimited with vertical dashed lines. The inset color-coded ± values are the standard deviation of the average diel cycle to provide an indicator of the variation.

In the floodplain, only the fluxes of CO_2 and CH_4 were measured. The average daily change of NEE was 12.5 µmol m^{-2} s^{-1} with predominant CO_2 uptake during the day (Figure 5h). The NEE was primarily influenced by light availability ($r^2 = 0.83$ to net radiation, $p < 0.05$). There was no evident diel cycle of FCH_{4_land}, as that observed in the riverine flux of CH_4 (Figure 5i), and FCH_{4_land} indicated no statistically significant correlation with any of the other analyzed parameters.

3.4. Dissolved Organic Matter (DOM) Characterization and Microbial Community Analyses

The solid-phase extraction of dissolved organic matter (DOM_{SPE}) at natural pH (~7.0) preventing hydrolysis reactions, revealed two distinct clusters related to the late freshet (**Phase 1**) and summer (**Phase 3**) samples after the sum formulae assignment (Figure 6a). In our study, *f*DOM and bulk DOC differed seasonally, with the highest values measured during the late freshet in **Phase 1** (100 QSU and DOC > 10 mg L^{-1}) and the lowest in summer in **Phase 3** (18.4 QSU and DOC < 10 mg L^{-1}) (Table S1 in Supporting Information S1). The elemental composition of the compounds identified in the DOM was comparable between the freshet and summer samples (inset figure, Figure 6a); however, the intensity of many compounds was different in each sample or some compounds were present only in one of the seasons (Figure 6b). We determined 492 sum formulae within the DOM signature, which were previously reported in samples from the Kolyma and Lena rivers (Dubinenkov et al., 2015; Spencer et al., 2015) (Figure S2 in Supporting Information S1).

The most identified compounds contained carbon, hydrogen, and oxygen (CHO; 58.1% in the late freshet, and 58.4% in summer); sum formula categories containing one or more heteroatoms were below 28%. Additionally,

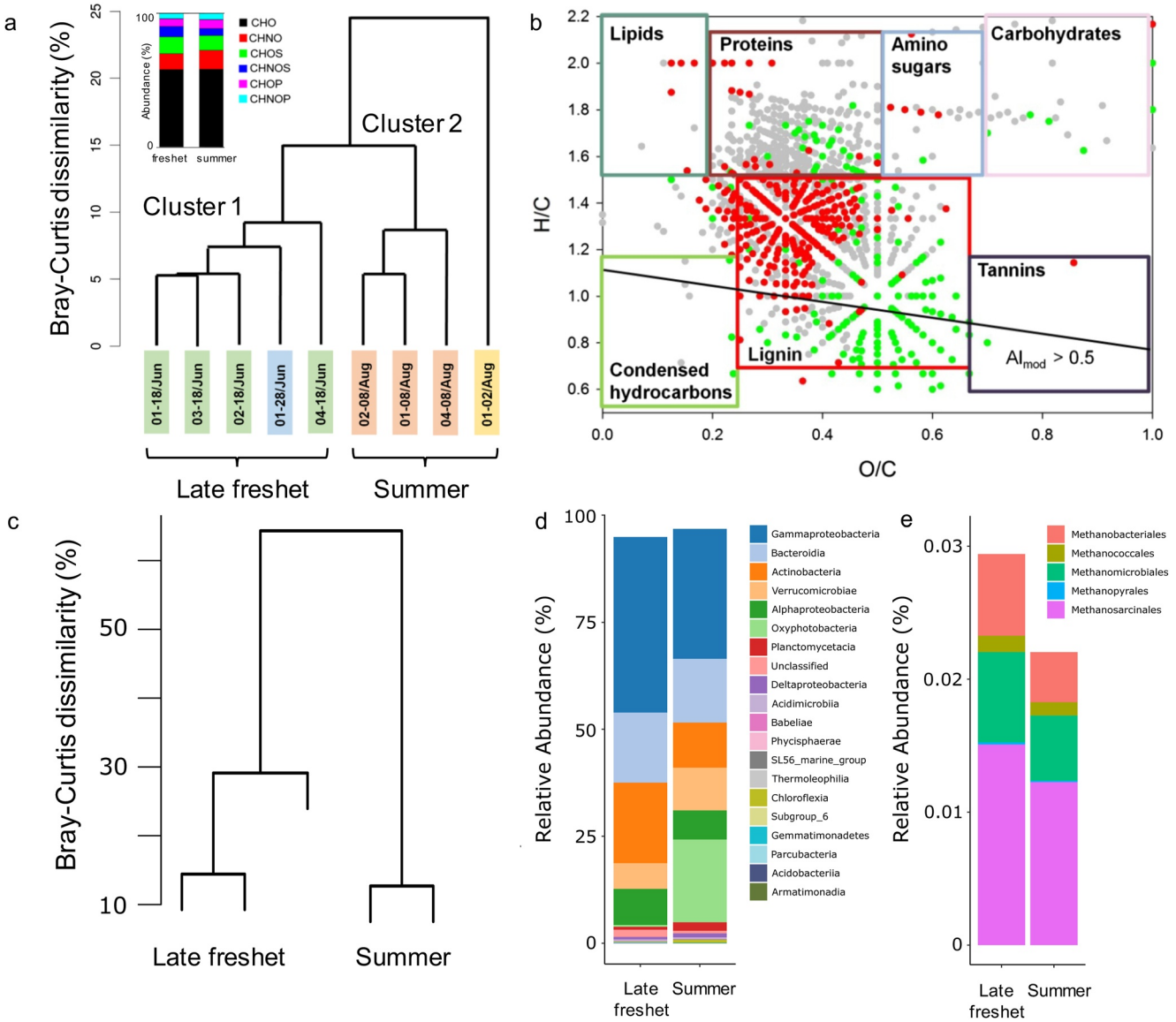

Figure 6. DOM_{SPE} and microbial composition analyses in discrete water samples. (a) Bray-Curtis dissimilarity of dissolved organic matter (DOM) fingerprints analysis in samples from the late freshet and summer in the Ambolikha River (inset, percentage distribution of elemental composition of the identified features, i.e., compounds). (b) van Krevelen diagram of the DOM_{SPE} groups with the classification of the compounds by H/C and O/C ratios and the modified aromatic indices (AI_{mod}). The specific biochemical sub-class ranges are shown based on the elemental ratios. Gray dots, core compounds; green dots, significantly different seasonal compounds in the late freshet, and red dots for summer. Only those compounds were considered, which were detected in all late freshet or summer samples (for details see the supporting text S.1.4.). Allocation of substance classes following Minor et al. (2014). (c) Bray-Curtis dissimilarity of the microbial composition analysis in samples. (d) relative abundance of microbial communities dominated by Gammaproteobacteria (29%–42%), Bacteriodia (14.9%–16.6%), Actinobacteria (9.8%–19.2%), Verrucomicrobiae (5.8%–10.4%), Alphaproteobacteria (6.6%–8.9%), and cyanobacteria (Oxyphotobacteria (0.3%–19.7%). (e) Abundances in the methanogen-containing order.

sulfur-containing compounds were more frequently detected during the late freshet period (inset figure, Figure 6a). Significant seasonal compounds (sSC, defined in the supplementary text S.1.6.) varying in abundance were found predominantly within the lignin-like substance class (Figure 6b). The late freshet samples that corresponded to the period with the highest *f*DOM contained a much higher proportion of aromatic compounds (indicated by the modified aromatic indices $AI_{mod} > 0.5$, Figure 6b) than the summer samples. Most of the DOM_{SPE} in our samples was classified into lignin-like substances, which overlapped with the carboxyl-rich alicyclic group (Figure 6b).

The microbial community composition in water samples revealed a seasonal shift from the late freshet (June) to summer (August) (two clusters shown in Figure 6c), similar to the variations observed in DOM_{SPE}, *f*DOM, and DOC. From the late freshet to summer, the relative abundance of Actinobacteria decreased, whereas the abundances of Oxyphotobacteria and Planctomycetaria increased (Figure 6d). Archeal 16S rRNA gene abundances measured using quantitative polymerase chain reaction (qPCR) were three to four orders of magnitude lower than bacterial 16S gene abundances within both the late freshet and summer samples. Archeal abundances significantly decreased between 18 June 2019 (discrete sample from **Phase 1**) and 8 August 2019 (discrete sample from **Phase 3**), from $(2.2 \pm 0.61) \times 10^7$ to $(7.0 \pm 2.6) \times 10^6$ gene copies L^{-1}, while bacterial abundances remained unchanged at $(6.9 \pm 1.5) \times 10^{10}$ gene copies L^{-1}. The 16S amplicon data exhibited the same pattern as the qPCR. Archeal sequences represented 0.02% of the total community in June (**Phase 1**) and were undetectable at our sequencing depth in August (**Phase 3**). The taxonomic characterizations of the two metagenomes were reflected in the 16S amplicon datasets, although the higher sequencing depths allowed for a better estimation of the relative abundances of groups affiliated with methanogenic archaea. Methanosarcinales was the most relatively abundant methanogen-containing order at both points in time (0.015% in **Phase 1**, and 0.012% in **Phase 3**) (Figure 6e).

3.5. Cumulative River and Floodplain Carbon Fluxes

The total cumulative riverine CO_2 emissions during the study were 36.8 gC-CO_2 m^{-2}, 0.21 gC-CH_4 m^{-2} for CH_4 (Table 1), and −81.8 gO_2 m^{-2} for FO_2 (i.e., 60.6 gC-O_2 m^{-2} as FCO_{2RQ}). During our study period, the CH_4 emission rates contributed to 0.6% of the total fluvial carbon emission rates (i.e., $FCO_2 + FCH_4$) from the ARS. We noted that the variations in the water residence time influenced the flux rate of the gases at the ARS, such that 66%–67% of the total CO_2 and CH_4 emissions during the study period occurred during **Phase 1**. The intermittent reversal of the water flow during **Phases 2** and **3** limited the exchange of the river water with gas-rich waters and slowed down the gas emissions at the ARS. In **Phases 2** and **3**, the remaining 18% and 16%, respectively, were emitted as FCO_2, whereas for FCH_4 it was 28% and 5%, respectively. As for FO_2, the sink of this gas at the ARS was largest during **Phase 1** (58% of the total FO_2 during the study), and this decreased during the last two phases (by 20% and 22% during **Phases 2** and **3**, respectively, of the total FO_2). The total cumulative riverine CO_2 emissions were equivalent to 22% of the CO_2 uptake (NEE) and 36% of the CO_2 emissions (i.e., from ecosystem respiration) at the floodplain site. As for CH_4, the total riverine emissions were equivalent to 6.4% of the emissions of the same gas from the floodplain site (FCH_{4_land}) (Table 1).

4. Discussion

4.1. Influence of Water Flow Regime on Emissions of Riverine Gases

Our continuous 38-day in situ measurements at a site in the Ambolikha River revealed large supersaturations of pCO_2 and pCH_4 (and O_2 undersaturation) that decreased steadily from the late freshet to summer (Figure 2). Changes in the water discharge can affect the advection of upstream or lateral carbon sources (Jones et al., 2017) in a river corridor, along with the riverine concentrations of CO_2 and CH_4 (Borges et al., 2018; Campeau & del Giorgio, 2014). In our study, 67% of the total riverine CO_2 and CH_4 emissions and O_2 uptake at the ARS occurred during the first two weeks of the study period, during the downstream high-flow period in the late freshet. The high-flow high-gas emissions response observed in our study can be attributed to the influence of the turbulent flow on the gas transfer velocity, as previously reported in rivers and streams in the Unites States of America (Liu & Raymond, 2018). The largely supersaturated riverine pCO_2 and pCH_4 during the late freshet could have been sustained primarily by external sources from downstream-flowing gas-rich headwaters or lateral export of these gases from terrestrial sources (e.g., surface runoff and active layer groundwater contributions) from the floodplain. At the freshet peak of flow discharge, the inundated floodplain from snowmelt runoff merged with the banks of the Ambolikha River, enhancing the lateral transport of terrestrial OM, gases, and organisms into the river channel. Through this study, we could show that the inversions in the flow direction were an additional element in the water flow regime that controlled the C-gas emissions and carbon assimilation at the ARS. As the flow regime (speed and direction) changed and the residence times of the water increased, this lotic system was transformed into a more stagnant inland water body during the summer basal flow, from mid-July to the end of the study period. This resulted in lower riverine CO_2 and CH_4 concentrations and emissions, as well as an increase in DO and reduction in the O_2 uptake (Figures 2 and 3) during the second half of the study, offering new opportunities for biogeochemical processing of the available carbon in the water.

4.2. Controlling Factors for Changes in Water Flow Regime of Ambolikha River

The variations in the water flow regime of a river can be associated with the modulation of water mass by natural processes or damming. Damming can alter the biotic habitats and carbon cycle of rivers significantly (Maavara et al., 2017; Vitousek et al., 1997). The water level in the Kolyma watershed is regulated by reservoirs for flood control during summer and power generation during winter (Majhi & Yang, 2008). During our study period, two potential mechanisms could have influenced the changes in the hydrological regime of Ambolikha River: first, the larger-scale daily discharge changes in the Kolyma River (registered at the Kolymsk-1 station) regulated the discharge variability in the Ambolikha River (positive linear correlation between daily Q averages, $r^2 = 0.70$; $p < 0.05$; Figure S3 in Supporting Information S1); second, the northward wind direction shifted to the southwest during the evening of 16 July 2019, with the upstream Q shift between 16–21 July 2019, in the ARS. In addition, semidiurnal Arctic Ocean tidal forces could further alter the river flow regime within small-order tributaries approximately 150 km upstream of the Kolyma estuary; however, observational evidence in the eastern shelf of the Arctic Ocean at the Laptev Sea indicated that these forces were rather weak (Janout & Lenn, 2014).

4.3. Biogeochemical Processing Signals in the River

Long river water residence times can limit the transport and exchange of water and carbon in small streams (Jones et al., 2017). At the same time, this enables the retention of pre-existing DOC within the channel leading to increased biogenic production of CO_2 and CH_4 (Campeau & del Giorgio, 2014). Our results indicated that in the ARS, inversions of the water flow diminish the replenishment of C-gases by limiting the downstream transport of gas-rich waters. Thus, surface evasion dominated, and the concentration of CO_2 and CH_4 depleted over time. However, the available carbon can also be buried in the river sediments during the low baseflow or assimilated for biomass storage during biogeochemical processing (Battin et al., 2009).

Thanks to our high-temporal resolution measurements at the ARS, we identified diel cycles that allow a closer investigation into the river metabolism and the biogeochemical carbon processing. These patterns have been observed previously in other river systems of the world (Nimick et al., 2011; Reiman & Xu, 2019; Rocher-Ros et al., 2019). The in-stream photosynthetic uptake of CO_2 by phytoplankton and subsequent production of O_2 might be depicted by the daytime increase of the latter at the ARS (Figure 5c). Despite the potential CO_2 uptake, the diel cycle of pCO_2 indicated a moderate increase during the day (Figure 5d), which might be linked to contributions from external lateral sources (i.e., surface or groundwaters, hinted by the positive correlation to specific conductivity), or local photochemical oxidation of terrestrial-DOC during the period of maximum net radiation (Figure 5a).

If the river DO variability was mostly driven by biological processes (i.e., balance between primary production and respiration), then, a portion of the daytime DO increase could be from the biological assimilation of CO_2 originated from the degradation of terrestrially derived organic substances. The average photosynthesis/respiration ratio (P/R, i.e., FC-O_2/FC-CO_2) was 1.6, and it increased over time from **Phase 1** (1.4) to **Phase 2** (1.8) and **Phase 3** (2.3). An increasing P/R ratio over time could be attributed to the increasing local CO_2 assimilation and O_2 production over time. However, at the ARS, the aquatic photosynthetic O_2 production was limited (despite the increased O_2 concentration from the late freshet to summer), in comparison to the excess emissions of CO_2. The P/R changes were most likely modulated by temporal variations in external CO_2 inputs (i.e., the hydraulic connectivity between the floodplain and the river [at the surface or via groundwaters]) and limited exchange with CO_2-rich waters. Also, internal factors played an important role in the changes in P/R; larger production of CO_2 from the bacterial use of organic compounds originated from the land, in situ photochemical degradations during the freshet, or CO_2 locally produced from CH_4 oxidation. Future studies need to evaluate the respiratory quotient (RQ) in Arctic rivers for a better understanding of the metabolic balance and contribution of external inputs over extended periods.

The presence and daytime increase of TAlgae concentrations seemed to be directly linked to the increasing daytime DO concentrations (Figure 5c), which could be related to photosynthetic O_2 production. However, this evidence is inconclusive given that the optical TAlgae measurements did not consider effects due to variations in the daylight during the diel cycle, which could influence the algal fluorescence response. Therefore, it is unclear how strongly the incident light interfered with the measurements of TAlgae. Also, high turbidity limits the light penetration in the water column and the development of phytoplankton blooms. We observed that in some periods

of our time series, the TAlgae concentration decreased as turbidity increased (Figure 2c); however, this was not always the case and the changes in turbidity were more related to changes in parameters, such as Q and κ, at a time scale larger than the daily cycle. Previous studies have provided evidence of the presence of phytoplankton blooms (dominated by diatoms and picocyanobacterial) in Arctic Rivers during the summer low flow, for example, in Lena River (Sorokin & Sorokin, 1996). After our measurement campaign, a green phytoplankton bloom was observed on 8 August 2019, at the confluence between the Pantheleika and Ambolikha rivers. At this site, we measured a maximum of TAlgae at 50-cm depth, with 30 μg L^{-1} in chl a (i.e., double than the maximum values measured at the ARS during the study period) (Figure 2). Detailed quantification of phytoplankton biomass or aquatic primary productivity is necessary to assess the photosynthetic carbon uptake and sink in aquatic biomass.

4.4. Shift in Dissolved Organic Matter (DOM) Composition and Role of Bacteria to the Presence of CO_2 and CH_4

The amount and composition of DOM in streams result from several sources and biogeochemical processing, such as biological production and photochemical degradation. In contrast to summer, we measured during the late freshet the highest *f*DOM and DOC concentrations and lowest κ (Figure 2; Table S1 in Supporting Information S1). Our findings agree with previously reported DOC values from a stream draining a Kolyma floodplain catchment (9.1–17.1 mg L^{-1}) (Mann et al., 2012).

The characterization of changes in DOM using molecular formula information revealed a significant difference between late freshet and summer samples (Figure 6), potentially due to the varying sources, including contributions from permafrost thawing. It is important to note that the sample preparation for the DOM analysis was carried out at natural pH (∼7.0) in order to minimize the potential for additional hydrolysis reactions that would lead to the additional formation of other types of compounds.

In general, small Arctic streams have a higher potential to contain P-DOM than main river channels (Mann et al., 2015; Spencer et al., 2015; Stubbins et al., 2017; Vonk et al., 2013, 2015). In the Ambolikha River, the hydraulic connectivity, permafrost thaw drainage, and in-stream microbial activity might have influenced the seasonal shift in the molecular signature of DOM. In the late freshet, we identified an elevated amount of sulfur polyoxygenated organic (CHOS) compounds and lignins that are characteristic of plant-derived organic matter (Hertkorn et al., 2006; Rossel et al., 2013) (Figure 6a). The CHOS compounds can be also produced in the presence of reduced sulfide species and lignin-like CHO compounds (Melendez-Perez et al., 2018). Because lignins may have been laterally supplied from the soil to the river during the high-flow periods (Dao et al., 2018; Feng et al., 2017), the composition of lignins shifted from the late freshet to summer (Figure 6b). In addition, physicochemical and biological decomposition processes contributed to the dynamic changes of lignins, independent of their origin in the ARS. However, as previously described (Kirby, 2005), our results suggest that actinobacteria may have played an important role in lignin degradation during the flood period from the late freshet to summer. Indeed, actinobacteria were one of the most common phyla found in the water samples, indicating constant absolute bacterial abundances over time. During the late freshet, actinobacteria ranked third (relative abundance of 18.8 ± 0.4%) and decreased to the fifth most abundant bacteria by summer (10.5 ± 1.0%) (Figure 6d).

In addition, iron can mediate the rapid photomineralization of lignin-rich P-DOM contributing further to the production of CO_2 in the Arctic Rivers (Bowen et al., 2020). The quality of DOM can be an important predictor of CO_2 concentrations in streams; elevated CO_2 levels can be found in the presence of complex terrestrial-DOM (D'Amario & Xenopoulos, 2015). In this context, large P-DOM fractions in Arctic rivers were reported as highly labile (Bowen et al., 2020; Spencer et al., 2015). In the samples of our study, the presence of P-DOM could be deduced from previously reported molecular formulae from samples of the Kolyma and Lena rivers (Dubinenkov et al., 2015; Spencer et al., 2015). However, no explicit distinction could be made for the dominant occurrence of contemporary P-DOM in the Ambolikha River late freshet and summer samples obtained in our study. Particularly, a specific analysis of a permafrost sample from the Ambolikha floodplain would have been necessary as a control sample for these molecular indicators, to corroborate the presence of and seasonal variations in the P-DOM in the river water.

Notably, more organic material was delivered into the Ambolikha River during the late freshet, and more carbon sources were available for microbial and photochemical decomposition when the net incoming radiation and wa-

ter temperature were increasing. As a result, riverine CO_2 concentrations (and CO_2 emissions to the atmosphere) were higher during the first days of the time series, as revealed by our findings.

The observed shift in bacterial communities from the late freshet to summer (Figure 6c) was in agreement with previous studies on bacterial seasonal shifts in Arctic rivers (Crump et al., 2009). Our analysis focused on the distribution and abundances of methanogens in the water samples, which could provide evidence of lateral transfers exporting bacteria and CH_4 from the soil to the river during the sampling periods. At the ARS, few methanogenic orders were detectable in the river water, and their low abundance declined significantly from the late freshet to summer. The source of the obligate anaerobic methanogens in the oxic river water was most likely due to groundwater discharge from the active layer via lateral export. The production rate of CH_4 and CO_2 were similar during long-term incubations of water-saturated thawed permafrost soils, under anoxic conditions (Knoblauch et al., 2018). Therefore, there is a high potential for increased CH_4 production in permafrost ecosystems in response to global warming. During the late freshet, the majority of the large CH_4 emissions in the water may have persisted mostly due to surface water connectivity. During summer, groundwater discharge is highly relevant at the peak of active layer thaw, when the flow in rivers is at its minima. Therefore, most of the CH_4 found in Arctic rivers and streams during summer may have originated from deeper soil layers, thus, sustaining the summer aquatic CH_4 emissions (Figures 2 and 3) (Connolly et al., 2020; van Grinsven et al., 2021; Harms et al., 2020; Olid et al., 2021). Because we did not measure the concentration of CH_4 just above the river bed, we could not account for the potential CH_4 efflux from anoxic hyporheic sediments into the water column.

4.5. Comparison of River and Floodplain Carbon Fluxes

The prevailing O_2 sink and CO_2 emissions at the ARS indicated predominant net heterotrophy. In contrast to the gas concentrations, the riverine diel cycles of FO_2 and FCO_2 (Figures 5g and 5h) were strongly modulated by changes in the gas solubility, due to temperature variations and the balance between carbon uptake (photosynthesis) and production (respiration). Notably, the ARS remained largely in an imbalanced metabolic state during our study period, with predominant CO_2 losses from respiration and gas exchange with the atmosphere, indicated by the long-term decrease of aquatic FCO_2 (Figure 3a). In contrast, the CO_2 uptake by terrestrial plants (NEE) in the floodplain dominated the carbon sink in this net autotrophic system. The land CO_2 uptake was nearly five times higher, and in the opposite direction, compared to the total in-stream CO_2 emissions. The land fluxes of CO_2 remained consistent throughout the study (Figure 4a) because they were primarily influenced by the light incidence cycle and represented a wet tussock tundra after weeks of the peak freshet. The total floodplain CH_4 emissions during the study period were higher than the CH_4 emitted from the river by sixteen-fold, corroborating the relevance of CH_4 production in Arctic wetlands despite the large and persistent riverine CH_4 supersaturations. Notably, the supersaturated CH_4 concentrations measured in the river water provide contemporary evidence of the source and fate of this gas in permafrost ecosystems. These findings highlight the importance of increasing the measurements of C-gases in Arctic inland waters that are subject to the effects of changes in the climate and adequately include them in carbon budgets.

4.6. Carbon Gas (C-gas) Concentrations and Fluxes Reported in Previous Studies in Arctic Rivers

Lower-order streams typically have higher gas concentrations than main stems of rivers due to their close proximity to groundwater gas sources (i.e., from the ground and shores) in narrower and shallower rivers (Raymond et al., 2012, 2013). In this context, the pCO_2 measured previously in the tributaries of Kolyma River was six-fold higher than that measured in the main river channel (Denfeld et al., 2013). The average pCO_2 measured at a site in the Ambolikha River during the summer of 2010 during low flow was 707 µatm (Denfeld et al., 2013). This value is comparable to the 536 µatm of pCO_2 measured at the ARS under similar conditions (during low flow) at the end of our study period. However, this value was only half of our average value for the entire time series data (Table 1).

We also compared our measurements with the data reported for the Yukon, Kuparuk, and Toolik rivers in North America (Kling et al., 1992; Rocher-Ros et al., 2020; Striegl et al., 2012) and in tributaries of Lena River (Vorobyev et al., 2021). Our pCO_2 values at the ARS were comparable to point-measurements from the Yukon River but were double the values reported in Kuparuk River of Alaska. The FCO_2 values at the ARS were in good agreement with most of the data reported in the compared studies in Arctic rivers, except for the fluxes measured

in Kuparuk River (Table 2). Mostly, the differences in water-to-air flux densities between our fluxes and those reported in other studies were due to varying gas transfer velocities and sampling dates. Therefore, these factors must be considered when comparing the data from different rivers (Table 2). Even if the flux differences were attributed to k_n, the majority of the measurements done in previous studies in Arctic rivers represented one-time-point samples collected during high-flow events over several years. These discrepancies prove the need for high temporal resolution measurements, to improve these estimates and avoid over or under-estimations of gas concentrations and fluxes in dynamic river systems.

4.7. Comparison of Gas Transfer Velocities to Other Aquatic Systems

Because the flow in the Ambolikha River system modified its behavior throughout the study from a lotic to lake-like ecosystem, it was difficult to choose one single k_n parameterization to effectively represent this system during the entire study period. Therefore, we chose to calculate k_n using four different methods. In a comparative analysis, k_n calculated with a wind-marine and wind-lake parameterizations (k_{W14} and k_{CC98}) were four to five times smaller than the k_n values reported in previous studies on Arctic rivers obtained using floating chambers to measure point CO_2 diffusion rates (Denfeld et al., 2013; Striegl et al., 2012) (Table 2). k_{W14} and k_{CC98} were also three times smaller than the estimated median value of 3 m d^{-1} for <60–100-m wide channels (Aufdekampe et al., 2011), which is also the mean value estimated for large rivers from modeling results across the world (Raymond et al., 2013).

In general, uncertainties in the calculation of gas emissions in aquatic ecosystems can be up to to 20% during the calculation of k_n (Wanninkhof, 2014). Our analysis with multiple k_n models, reveals that the emission of fluxes can differ up to two orders of magnitude in relation to the use of different k_n values (Figures 3a and 3b), and this is particularly evident in periods where the concentration of dissolved gases is higher (i.e., during late freshet). Because the gas transfer velocities in the main river channel of larger streams tend to be greater than that in small rivers and streams (Raymond et al., 2013), the comparison of k_n values obtained in different studies must consider the morphology of the study sites. In addition, other uncertainties in the water gas flux estimations arise from explicitly unaccounted contributions of POC and DOC released from the land into the channel and DO changes due to turbulent physical processes. The large variations in k_n values reported in the literature suggest the need for k_n to be measured more accurately and consistently across the spectrum of freshwater systems, for more reliable determination and comparison of gas fluxes. Nevertheless, the estimated k_n values from empirical parameterizations provide a good proxy for the calculation of gas emissions and comparison to different areas and/or studies.

5. Conclusions

In this study, we revealed high temporal variations in CO_2 and CH_4 fluxes from an Arctic stream, influenced by the seasonal changes of the hydrological regime. Decreasing water discharge from the freshet to summer and persistent reversals in the water flow direction cause the water to remain in the channel, limiting lateral exchange with gas-rich downstream or upstream flowing water. In general, during the freshet, the hydraulic connectivity between the Arctic land and streams is enhanced. Additionally, permafrost thaw accelerates the formation of groundwater drainage, promoting the availability of organic substances and preformed terrestrial gases to the environment. In the Ambolikha River, during the late freshet, we measured high CO_2 and CH_4 concentrations, accompanied by a higher abundance of methanogens and the signal of labile terrestrial organic matter, which might have been exported laterally into the stream during hydraulic connectivity, influencing the microbiome's productivity. DOM that drives bacterial respiration was primarily derived from the decomposition of plants and permafrost material and contained many thousands of organic molecules broken down by bacteria at various time scales. Future studies can shape our understanding of how specific DOM molecules influence bacterial respiration, to forecast the carbon cycle across the land-permafrost-water continuum.

Interestingly, this replenishment process accelerates the formation and directs large riverine emissions of CO_2 and CH_4 to the atmosphere. Therefore, Arctic flowing waters can become effective vectors for atmospheric emissions of terrestrial C-gases, particularly during the high-flow periods. As the flow rate slows down, it provides opportunities for in-stream biogeochemical processing and storage of carbon during the summer low-flow, further impacting local primary productivity.

Although the magnitude of terrestrial CO_2 uptake and CH_4 emissions were higher than the riverine emissions, our study indicated the importance of long-term monitoring with high-temporal resolution of carbon gas sources and sinks in Arctic inland waters for better quantification and assessment of future changes under warming conditions. Notably, to assess the current knowledge gaps, it is necessary to consider the importance of the hydraulic connectivity and variations in the fluvial hydrological regime across different temporal and spatial scales in Arctic streams and rivers. This is critical for accurately calculating the contribution of these Arctic water bodies to global carbon budgets and improving our understanding of how they are affected by climate change.

Conflict of Interest

The authors declare no conflicts of interest relevant to this study.

Data Availability Statement

Data sets presented and used for the artwork contained in this manuscript related to the water and floodplain measurements and analysis of dissolved organic matter can be found in the Zenodo EU data repository under the following link: https://doi.org/10.5281/zenodo.5758728. The microbiology data can be accessed in: https://www.ebi.ac.uk/ena/browser/view/PRJEB43451?show=reads

Acknowledgments
This work was conceived and developed within the project PROPERAQUA funded by the Deutsche Forschungsgemeinschaft (DFG, German Research Foundation) with number 396657413. The contributions from AC and AK were funded by the C-CASCADES ITN of the EU (project number 643052), and the MOSES program of the Helmholtz Association. MG and OK were supported through funding by the European Commission (INTAROS project, No. 727890 and Nunataryuk project, No. 773421), and the German Ministry of Education and Research (KoPf project, Grant No. 03F0764D). KK and WAO were supported by the Collaborative Research Centre 1076 AquaDiva (CRC AquaDiva) funded by DFG (project No. ID 218627073). TW and SR were funded by the DFG in the framework of the priority program (SPP 1158) "Antarctic Research with comparative investigations in Arctic ice areas" (project No. 424256657). The authors thank the personnel of the Northeast Scientific Station and Pleistocene Park in Chersky for their valuable assistance during the field work, as well as Dr. Robert Lehmann for the analysis of DOC samples at the FSU. Many thanks to two anonymous reviewers for their helpful comments and critical reading throughout the revision of this work. Open access funding was enabled and organized by Projekt DEAL.

References

Abril, G., & Borges, A. V. (2019). Ideas and perspectives: Carbon leaks from flooded land: Do we need to replumb the inland water active pipe? *Biogeosciences*, *16*, 769–784. https://doi.org/10.5194/bg-16-769-2019

Amorocho, J., & Devries, J. J. (1980). A new evaluation of the wind stress coefficient over water surfaces. *Journal of Geophysical Research*, *85*(C1), 433–442. https://doi.org/10.1029/JC085iC01p00433

Aufdekampe, A. K., Mayorga, E., Raymond, P. A., Melack, J. M., Doney, S. C., Alin, S. R., et al. (2011). Riverine coupling of biogeochemical cycles between land, oceans, and atmosphere. *Frontiers in Ecology and the Environment*(9), 53–60. https://doi.org/10.1890/100014

Battin, T. J., Luyssaert, S., Kaplan, J. O., Aufdekampe, A. K., Richter, A., & Tranvik, L. J. (2009). The boundless carbon cycle. *Nature Geoscience*, *2*, 598–600. https://doi.org/10.1038/ngeo618

Berggren, M., Lapierre, J.-F., & del Giorgio, P. A. (2012). Magnitude and regulation of bacterioplankton respiratory quotient across freshwater environmental gradients. *The ISME Journal*, *6*, 984–993. https://doi.org/10.1038/ismej.2011.157

Borges, A. V., Darchambeau, F., Lambert, T., Bouillon, S., Morana, C., Brouyère, S., et al. (2018). Effects of agricultural land use on fluvial carbon dioxide, methane and nitrous oxide concentrations in a large European river, the Meuse (Belgium). The *Science of the Total Environment*, *610–611*, 342–355. https://doi.org/10.1016/j.scitotenv.2017.08.047

Bowen, J. C., Ward, C. P., Kling, G. W., & Cory, R. M. (2020). Arctic amplification of global warming strengthened by sunlight oxidation of permafrost carbon to CO_2. *Geophysical Research Letters*, *47*, 1–8. https://doi.org/10.1029/2020GL087085

Broderick, D. E., Frey, K. E., Rogan, J., Alexander, H. D., & Zimov, N. (2015). Estimating upper soil horizon carbon stocks in a permafrost watershed of Northeast Siberia by integrating field measurements with Landsat-5 TM and WorldView-2 satellite data. *GIScience and Remote Sensing*, *52*(2), 131–157. https://doi.org/10.1080/15481603.2015.1010434

Campeau, A., & del Giorgio, P. A. (2014). Patterns in CH_4 and CO_2 concentrations across boreal rivers: Major drivers and implications for fluvial greenhouse emissions under climate change scenarios. *Global Change Biology*, *20*, 1075–1088. https://doi.org/10.1111/gcb.12479

Canning, A., Körtzinger, A., Fietzek, P., & Rehder, G. (2021). Technical note: Seamless gas measurements across land-ocean aquatic continuum - Corrections and evaluation of sensor data for CO_2, CH_4 and O_2 from field deployments in contrasting environments. *Biogeosciences*, *18*, 1351–1373. https://doi.org/10.5194/bg-18-1351-2021

Cochrane, D., & Orcutt, G. H. (1949). Application of least squares regression to relationships containing autocorrelated error terms. *Journal of the American Statistical Association*, *44*, 32–61

Cole, J. J., & Caraco, N. F. (1998). Atmospheric exchange of carbon dioxide in a low-wind oligotrophic lake measured by the addition of SF_6. *Limnology & Oceanography*, *43*(4), 647–656. https://doi.org/10.4319/lo.1998.43.4.0647

Cole, J. J., Prairie, Y. T., Caraco, N. F., McDowell, W. H., Tranvik, L. J., Striegl, R. G., et al. (2007). Plumbing the global carbon cycle: Integrating inland waters into the terrestrial carbon budget. *Ecosystems*, *10*, 171–184. https://doi.org/10.1007/s10021-006-9013-8

Connolly, C. T., Cardenas, M. B., Burkart, G. A., Spencer, R. G. M., & McClelland, J. W. (2020). Groundwater as a major source of dissolved organic matter to Arctic coastal waters. *Nature Communications*, *11*(1479), 1–8. https://doi.org/10.1038/s41467-020-15250-8

Cory, R. M., Ward, C. P., Crump, B. C., & Kling, G. W. (2014). Sunlight controls water column processing of carbon in arctic fresh waters. *Science*, *345*(6199), 925–928. https://doi.org/10.1126/science.1253119

Covino, T. (2017). Hydrologic connectivity as a framework for understanding biogeochemical flux through watersheds and along fluvial networks. *Geomorphology*, *277*, 133–144. https://doi.org/10.1016/j.geomorph.2016.09.030

Crump, B. C., Peterson, B. J., Raymond, P. A., Amon, R. M. W., Rinehart, A., McClelland, J. W., & Holmes, R. M. (2009). Circumpolar synchrony in big river bacterioplankton. *Proceedings of the National Academy of Sciences of the United States of America*, *106*(50). https://doi.org/10.1073/pnas.0906149106

D'Amario, S. C., & Xenopoulos, M. A. (2015). Linking dissolved carbon dioxide to dissolved organic matter quality in streams. *Biogeochemistry*, *126*, 99–114. https://doi.org/10.1007/s10533-015-0143-y

Dao, T. T., Gentsch, N., Mikutta, R., Sauheitl, L., Shibistova, O., Wild, B., et al. (2018). Fate of carbohydrates and lignin in north-east Siberian permafrost soils. *Soil Biology and Biochemistry*, *116*, 311–322. https://doi.org/10.1016/j.soilbio.2017.10.032

Dean, J. F., Meisel, O. H., Martyn, R. M., Belelli, L. M., Garnett, M. H., Lenderink, H., et al. (2020). East Siberian Arctic inland waters emit mostly contemporary carbon. *Nature Communications*, *11*, 1627. https://doi.org/10.1038/s41467-020-15511-6

Denfeld, B. A., Frey, K. E., Sobczak, W. V., Mann, P. J., & Holmes, R. M. (2013). Summer CO_2 evasion from streams and rivers in the Kolyma River basin, north-east Siberia. *Polar Research*, *32*, 19704. https://doi.org/10.3402/polar.v32i0.19704

Dlugokencky, E. (2019). NOAA/GML. Retrieved from www.esrl.noaa.gov/gmd/ccgg/trends_ch4/

Dlugokencky, E. & Tans, P. P. (2019). Retrieved from www.esrl.noaa.gov/gmd/ccgg/trends/

Downing, B. D., Pellerin, B. A., Bergamaschi, B. A., Saraceno, J. F., & Kraus, T. E. C. (2012). Seeing the light: The effects of particles, dissolved materials, and temperature on in situ measurements of DOM fluorescence in rivers and streams. *Limnology and Oceanography: Methods*, *10*, 767–775. https://doi.org/10.4319/lom.2012.10.767

Dubinenkov, I., Flerus, R., Schmitt-Kopplin, P., Kattner, G., & Koch, B. P. (2015). Origin-specific molecular signatures of dissolved organic matter in Lena Delta. *Biogeochemistry*, *123*, 1–14. https://doi.org/10.1007/s10533-014-0049-0

Feng, X., Vonk, J. E., Griffin, C. G., Zimov, N., Montluçon, D. B., Wacker, L., & Eglinton, T. I. (2017). ^{14}C variation of dissolved lignin in Arctic river systems. *ACS Earth Space Chemistry*, *1*(6), 334–344. https://doi.org/10.1021/acsearthspacechem.7b00055

Fichot, C. G., Kaiser, K., Hooker, S. B., Amon, R. M. W., Babin, M., Bélanger, S., et al. (2013). Pan-Arctic distributions of continental runoff in the Arctic Ocean. *Scientific Reports*, *3*(1053), 1–6. https://doi.org/10.1038/srep01053

Fietzek, P., Fiedler, B., Steinhoff, T., & Körtzinger, A. (2014). In situ quality assessment of a novel underwater pCO_2 sensor based on membrane equilibration and NDIR spectrometry. *Journal of Atmospheric and Oceanic Technology*, *31*(1), 181–196. https://doi.org/10.1175/JTECH-D-13-00083.1

Fritz, M., Vonk, J. E., & Lantuit, H. (2017). Collapsing arctic coastlines. *Nature Climate Change*, *7*, 6–7. https://doi.org/10.1038/nclimate3188

Garcia, H. E., & Gordon, L. I. (1992). Oxygen solubility in seawater: Better fitting equations. *Limnology & Oceanography*, *37*(6), 1307–1312. https://doi.org/10.4319/lo.1992.37.6.1307

Göckede, M., Kittler, F., Kwon, M. J., Burjack, I., Heimann, M., Kolle, O., et al. (2017). Shifted energy fluxes, increased Bowen ratios, and reduced thaw depths linked with drainage-induced changes in permafrost ecosystem structure. *The Cryosphere*, *11*, 2975–2996. 10.5194/tc-11-2975-2017

Hall, R. O., & Ulseth, A. J. (2019). Gas exchange in streams and rivers. *WIREs Water*, *7*(1), 1–18. https://doi.org/10.1002/wat2.1391

Harmon, T. C. (2020). Carbon gas flux to and from inland waters: Support for a global observation network. *Limnology*, *21*(3), 429–442. https://doi.org/10.1007/s10201-020-00623-1

Harms, T. K., Rocher-Ros, G., & Goodsey, S. E. (2020). Emission of greenhouse gases from water tracks draining Arctic hillslopes. *Journal of Geophysical Research: Biogeosciences*, *125*, e2020JG005889. https://doi.org/10.1029/2020JG005889

Hertkorn, N., Benner, R., Frommberger, M., Schmitt-Kopplin, P., Witt, C., Kaiser, K., et al. (2006). Characterization of a major refractory component of marine dissolved organic matter. *Geochimica et Cosmochimica Acta*, *70*, 2990–3010. https://doi.org/10.1016/j.gca.2006.03.021

Hilbe, J. M. (2014). *Modeling Count data*. Cambridge University Press. https://doi.org/10.1017/CBO9781139236065

Hotchkiss, E. R., Hall, R. O., Sponseller, R. A., Butman, D., Klaminder, J., Laudon, H., et al. (2015). Sources of and processes controlling CO_2 emissions change with the size of streams and rivers. *Nature Geoscience*, *8*, 696–699. https://doi.org/10.1038/ngeo2507

Izagirre, O., Bermejo, M., Pozo, J., & Elosegi, A. (2007). RIVERMET(c): An Excel-based tool to calculate river metabolism from diel oxygen-concentration curves. *Environmental Modelling & Software*, *22*, 24–32. https://doi.org/10.1016/j.envsoft.2005.10.001

Janout, M., & Lenn, Y.-D. (2014). Semidiurnal tides on the Laptev Sea Shelf with implications for shear and vertical mixing. *Journal of Physical Oceanography*, *44*, 202–2019. https://doi.org/10.1175/JPO-D-12-0240.1

Jones, A. E., Hodges, B. R., McClelland, J. W., Hardison, A. K., & Moffett, K. B. (2017). Residence-time-based classification of surface water systems. *Water Resources Research*, *53*, 5567–5584. 10.1002/2016WR019928

Karlsson, J., Serikova, S., Vorobyev, S. N., Rocher-Ros, G., Denfeld, B. A., & Pokrovsky, O. S. (2021). Carbon emission from Western Siberian inland waters. *Nature Communications*, *12*(825), 1–8. https://doi.org/10.1038/S41467-021-21054-1

Kirby, R. (2005). Actinomycetes and lignin degradation. *Advances in Applied Microbiology*, *58*, 125–168. https://doi.org/10.1016/S0065-2164(05)58004-3

Kittler, F., Burjack, I., Corradi, C. A. R., Heimann, M., Kolle, O., Merbold, L., et al. (2016). Impacts of a decadal drainage disturbance on surface-atmosphere fluxes of carbon dioxide in a permafrost ecosystem. *Biogeosciences*, *13*, 5315–5332. https://doi.org/10.5194/bg-13-5315-2016

Kittler, F., Heimann, M., Kolle, O., Zimov, N., Zimov, S., & Göckede, M. (2017). Long-term drainage reduces CO_2 uptake and CH_4 emissions in a Siberian permafrost ecosystem. *Global Biogeochemical Cycles*, *31*, 1704–1717. https://doi.org/10.1002/2017GB005774

Kling, G. W., Kipphut, G. W., & Miller, M. C. (1991). Arctic lakes and streams as gas conduits to the atmosphere: Implications for tundra carbon budgets. *Science*, *251*, 298–301. https://doi.org/10.1126/science.251.4991.298

Kling, G. W., Kipphut, G. W., & Miller, M. C. (1992). The flux of CO_2 and CH_4 from lakes and rivers in arctic Alaska. *Hydrobiologia*, *240*, 23–26. https://doi.org/10.1007/BF00013449

Knoblauch, C., Beer, C., Liebner, S., Grigoriev, M. N., & Pfeiffer, E.-M. (2018). Methane production as key to the greenhouse gas budget of thawing permafrost. *Nature Climate Change*, *8*, 309–312. https://doi.org/10.1038/s41558-018-0095-z

Koch, B. P., Dittmar, T., Witt, M., & Kattner, G. (2007). Fundamentals of molecular formula assignment to ultrahigh resolution mass data of natural organic matter. *Analytical Chemistry*, *79*(4), 1758–1763. https://doi.org/10.1021/ac061949s

Kügler, S., Cooper, R. E., Wegner, C.-E., Mohr, J. F., Wichard, T., & Küsel, K. (2019). Iron-organic matter complexes accelerate microbial iron cycling in an iron-rich fen. The *Science of the Total Environment*, *646*, 972–988. https://doi.org/10.1016/j.scitotenv.2018.07.258

Leefmann, T., Frickenhaus, S., & Koch, B. P. (2019). UltraMassExplorer: A browser-based application for the evaluation of high-resolution mass spectrometric data. *Rapid Communications in Mass Spectrometry*, *33*(2), 193–202. https://doi.org/10.1002/rcm.8315

Liu, S., & Raymond, P. A. (2018). Hydrologic controls on pCO_2 and CO_2 efflux in US streams and rivers. *Limnology and Oceanography Letters*, *3*, 428–435. https://doi.org/10.1002/lol2.10095

Maavara, T., Lauerwald, R., Regnier, P. A. G., & Van Cappellen, P. (2017). Global perturbation of organic carbon cycling by river damming. *Nature Communications*, *8*(15347), 1–10. https://doi.org/10.1038/ncomms15347

Majhi, I., & Yang, D. (2008). Streamflow characteristics and changes in Kolyma basin in Siberia. *Journal of Hydrometeorology*, *9*(2), 267–279. https://doi.org/10.1175/2007JHM845.1

Mann, P. J., Davydova, A., Zimov, N., Spencer, R. G. M., Davydov, S., Bulygina, E., et al. (2012). Controls on the composition and lability of dissolved organic matter in Siberia's Kolyma River basin. *Journal of Geophysical Research*, *117*, G01028. https://doi.org/10.1029/2011JG001798

Mann, P. J., Eglinton, T. I., McIntyre, C. P., Zimov, N., Davydova, A., Vonk, J. E., et al. (2015). Utilization of ancient permafrost carbon in headwaters of Arctic fluvial networks. *Nature Communications*, *6*(7856), 1–7. https://doi.org/10.1038/ncomms8856

Melendez-Perez, J. J., Martinez-Mejia, M. J., Barcellos, R. L., Fetter-Filho, A. F. H., & Eberlin, M. N. (2018). A potential formation route for CHOS compounds in dissolved organic matter. *Marine Chemistry*, *202*, 67–72. https://doi.org/10.1016/j.marchem.2018.03.006

Meredith, M., Sommerkorn, M., Cassotta, S., Derksen, C., Ekaykin, A., Hollowed, A., et al. (2019). *Polar regions Rep*.
Minor, E. C., Swenson, M. M., Mattson, B. M., & Oyler, A. R. (2014). Structural characterization of dissolved organic matter: A review of current techniques for isolations and analysis. *Environmental Science: Processes & Impacts*, *16*(9), 2064–2079. https://doi.org/10.1039/c4em00062e
Nimick, D. A., Gammons, C. H., & Parker, S. R. (2011). Diel biogeochemical processes and their effect on the aqueous chemistry of streams: A review. *Chemical Geology*, *283*, 3–17. 10.1016/j.chemgeo.2010.08.017
Odum, H. T. (1956). Primary production in flowing waters. *Limnology & Oceanography*, *1*(2), 102–117. https://doi.org/10.4319/lo.1956.1.2.0102
Olid, C., Zannella, A., & Lau, D. C. P. (2021). The role of methane transport from the active layer in sustaining methane emissions and food chains in subarctic ponds. *Journal of Geophysical Research: Biogeosciences*, *126*, e2020JG005810. https://doi.org/10.1029/2020JG005810
Pringle, C. (2003). What is hydrologic connectivity and why is it ecologically important? *Hydrological Processes*, *17*, 2685–2689. https://doi.org/10.1002/hyp.5145
Raymond, P. A., Hartmann, J., Lauerwald, R., Sobek, S., McDonald, C., Hoover, M., et al. (2013). Global carbon dioxide emissions from inland waters. *Nature*, *503*, 355–359. https://doi.org/10.1038/nature12760
Raymond, P. A., McClelland, J. W., Holmes, R. M., Zhulidov, A. V., Mull, K., Peterson, B. J., et al. (2007). Flux and age of dissolved organic carbon exported to the Arctic Ocean: A carbon isotopic study of the five largest arctic rivers. *Global Biogeochemical Cycles*, *21*, GB4011. https://doi.org/10.1029/2007GB002934
Raymond, P. A., Zappa, C. J., Butman, D., Bott, T. L., Potter, J. D., Mulholland, P., et al. (2012). Scaling the gas transfer velocity and hydraulic geometry in streams and small rivers. *Limnology and Oceanography: Fluids and Environments*, *2*, 41–53. https://doi.org/10.1215/21573689-1597669
Regnier, P. A. G., Friedlingstein, P., Ciais, P., Mackenzie, F. T., Gruber, N., Janssens, I. A., et al. (2013). Anthropogenic perturbation of the carbon fluxes from land to ocean. *Nature Geoscience*, *6*, 597–607. https://doi.org/10.1038/NGEO1830
Reiman, J. H., & Xu, Y. J. (2019). Diel variability of pCO_2 and CO_2 outgassing from the lower Mississippi river: Implications for riverine CO_2 outgassing estimation. *Water*, *11*(43), 1–15. https://doi.org/10.3390/w11010043
Rocher-Ros, G., Harms, T. K., Sponseller, R. A., Väisänen, M., Mörth, C.-M., & Giesler, R. (2020). Metabolism overrides photo-oxidation in CO_2 dynamics of Arctic permafrost streams. *Limnology & Oceanography*, *66*(S1), 1–13. https://doi.org/10.1002/lno.11564
Rocher-Ros, G., Sponseller, R. A., Bergström, A.-K., Myrstener, M., & Giesler, R. (2019). Stream metabolism controls diel patterns and evasion of CO_2 in Arctic streams. *Global Change Biology*, *26*, 1400–1413. https://doi.org/10.1111/gcb.14895
Rossel, P. E., Vähätalo, A. V., Witt, M., & Dittmar, T. (2013). Molecular composition of dissolved organic matter from a wetland plant (Juncus effusus) after photochemical and microbial decomposition (1.25 yr): Common features with deep sea dissolved organic matter. *Organic Geochemistry*, *60*, 62–71. https://doi.org/10.1016/j.orggeochem.2013.04.013
Schuur, E. A., McGuire, D., Schädel, C., Grosse, G., Harden, J. W., Hayes, D. J., et al. (2015). Climate change and the permafrost carbon feedback. *Nature*, *520*, 171–179. https://doi.org/10.1038/nature14338
Shiklomanov, A. I., Holmes, R. M., McClelland, J. W., Tank, S. E. & Spencer, R. G. M. Arctic Great Rivers Observatory. Date of collection 1978-2020 (Version 20200713). https://www.arcticrivers.org/data
Shiklomanov, I. A., Shiklomanov, A. I., Lammers, R. B., Peterson, B. J., & Vorosmarty, C. J. (2000). The dynamics of river water inflow to the Arctic Ocean. In E. L. Lewis, E. P. Jones, P. Lemke, T. D. Prowse, & P. Wadhams (Eds.), *The freshwater budget of the Arctic Ocean. NATO Science series* (pp. 281–296). Springer. https://doi.org/10.1007/978-94-011-4132-1_13
Snyder, L., Potter, J. D., & McDowell, W. H. (2018). An evaluation of nitrate, fDOM, and turbidity sensors in New Hampshire Streams. *Water Resources Research*, *54*, 2466–2479. https://doi.org/10.1002/2017WR020678
Sorokin, Y. I., & Sorokin, P. Y. (1996). Plankton and primary production in the Lena river estuary and in the south-eastern Laptev Sea. *Estuarine, Coastal and Shelf Science*, *43*(4), 399–418. https://doi.org/10.1006/ecss.1996.0078
Spencer, R. G. M., Mann, P. J., Dittmar, T., Eglinton, T. I., McIntyre, C. P., Holmes, R. M., et al. (2015). Detecting the signature of permafrost thaw in Arctic rivers. *Geophysical Research Letters*, *42*, 2830–2835. https://doi.org/10.1002/2015GL063498
Stanley, E. H., Casson, N. J., Christel, S. T., Crawford, J. T., Loken, L. C., & Oliver, S. K. (2016). The ecology of methane in streams and rivers: Patterns, controls, and global significance. *Ecological Monographs*, *86*(2), 146–171. https://doi.org/10.1890/15-1027
Strauss, J., Schirrmeister, L., Grosse, G., Fortier, D., Hugelius, G., Knoblauch, C., et al. (2017). Deep yedoma permafrost: A synthesis of depositional characteristics and carbon vulnerability. *Earth-Science Reviews*, *172*, 75–86. https://doi.org/10.1016/j.earscirev.2017.07.007
Striegl, R. G., Dornblaser, M. M., McDonald, C. P., Rover, J. R., & Stets, E. G. (2012). Carbon dioxide and methane emissions from the Yukon River system. *Global Biogeochemical Cycles*, *26*, GB0E05. https://doi.org/10.1029/2012GB004306
Stubbins, A., Mann, P. J., Powers, L., Bittar, T. B., Dittmar, T., McIntyre, C. P., et al. (2017). Low photolability of yedoma permafrost dissolved organic carbon. *Journal of Geophysical Research: Biogeosciences*, *122*, 200–211. https://doi.org/10.1002/2016JG003688
Turetsky, M. R., Abbott, B. W., Jones, M. C., Walter Anthony, K., Olefeldt, D., Schuur, E. A., et al. (2020). Carbon release through abrupt permafrost thaw. *Nature Geoscience*, *13*, 138–143. https://doi.org/10.1038/s41561-019-0526-0
van Grinsven, S., Oswald, K., Wehrli, B., Jegge, C., Zopfi, J., Lehmann, M. F., & Schubert, C. J. (2021). Methane oxidation in the waters of a humic-rich boreal lake stimulated by photosynthesis, nitrite, Fe(III) and humics. *Biogeosciences*, *18*, 3087–3101. https://doi.org/10.5194/bg-18-3087-2021
Vitousek, P. M., Mooney, H. A., Lubchenco, J., & Melillo, J. M. (1997). Human domination of Earth's ecosystems. *Science*, *277*, 494–499. https://doi.org/10.1126/science.277.5325.494
Vonk, J. E., Mann, P. J., Davydov, S., Davydova, A., Spencer, R. G. M., Schade, J., et al. (2013). Hight biolability of ancient permafrost carbon upon thaw. *Geophysical Research Letters*, *40*, 2689–2693. https://doi.org/10.1002/grl.50348
Vonk, J. E., Tank, S. E., Mann, P. J., Spencer, R. G. M., Treat, C. C., Striegl, R. G., et al. (2015). Biodegradability of dissolved organic carbon in permafrost soils and aquatic systems: A meta-analysis. *Biogeosciences*, *12*, 6915–6930. https://doi.org/10.5194/bg-12-6915-2015
Vorobyev, S. N., Karlsson, J., Kolesnichenko, Y. Y., & Koretz, M. (2021). Fluvial carbon dioxide emission from the Lena River basin during spring flood. *Biogeosciences Discussions*. https://doi.org/10.5194/bg-2021-109
Wanninkhof, R. (1992). Relationship between gas exchange and wind speed over the ocean. *Journal of Geophysical Research*, *97*, 7373–7381. https://doi.org/10.1029/92JC00188
Wanninkhof, R. (2014). Relationship between wind speed and gas exchange over the ocean revisited. *Limnology and Oceanography: Methods*, *12*, 351–362. https://doi.org/10.4319/lom.2014.12.351
Ward, N. D., Bianchi, T. S., Medeiros, P. M., Seidel, M., Richey, J. E., Keil, R. G., & Sawakuchi, H. O. (2017). Where carbon goes when water flows: Carbon cycling across the aquatic continuum. *Frontiers in Marine Science*, *4*(7). https://doi.org/10.3389/fmars.2017.00007
Watras, C. J., Hanson, P. C., Stacy, T. L., Morrison, K. M., Mather, J., Hu, Y.-H., & Milewski, P. (2011). A temperature compensation method for CDOM fluorescence sensors in freshwater. *Limnology and Oceanography: Methods*, *9*(7), 296–301. https://doi.org/10.4319/lom.2011.9.296
Weiss, R. F. (1970). The solubility of nitrogen, oxygen and argon in water and sea water. *Deep Sea Research*, *17*, 721–735. https://doi.org/10.1016/0011-7471(70)90037-9

Weiss, R. F. (1974). Carbon dioxide in water and seawater: The solubility of a non-ideal gas. *Marine Chemistry*, *2*, 203–215. https://doi.org/10.1016/0304-4203(74)90015-2

Wiesenburg, D. A., & Guinasso, J. N. L. (1979). Equilibrium solubilities of methane, carbon monixide, and hydrogen in water and sea water. *Journal of Chemical & Engineering Data*, *24*, 356–360. https://doi.org/10.1021/cr60306a003

Wooldridge, J. M. (2013). *Introductory Econometrics: A modern approach*. South-Western, Cengage learning

Zolkos, S., Tank, S. E., Striegl, R. G., & Kokelj, S. V. (2019). Thermokarst Effects on Carbon Dioxide and Methane Fluxes in Streams on the Peel Plateau (NWT, Canada). *Journal of Geophysical Research: Biogeosciences*, *124*(7), 1781–1798. https://doi.org/10.1029/2019jg005038

References From the Supporting Information

Alsufyani, T., Weiss, A., & Wichard, T. (2017). Time course exo-metabolomic profiling in the green marine macroalga *Ulva* (Chlorophyta) for identification of growth phase-dependent biomarkers. *Marine Drugs*, *15*(1), 14. https://doi.org/10.3390/md15010014

Anderson, M., & Willis, T. (2003). Canonical analysis of principal coordinates: A useful method of constrained ordination for ecology. *Ecology*, *84* 5112–5525. https://doi.org/10.1890/0012-9658(2003)084

Anderson, M. J., & Robinson, J. (2003). Generalized discriminant analysis based on distances. *Australian & New Zealand Journal of Statistics*, *45*(3), 301–318. https://doi.org/10.1111/1467-842X.00285

Bushnell, B. (2014). *BBTools Software package*.

Callahan, B. J., McMurdie, P. J., Rosen, M. J., Han, A. W., Johnson, A. J. A., & Holmes, S. P. (2016). DADA2: High-resolution sample interference from Illumina amplicon data. *Nature Methods*, *13*, 581–583. https://doi.org/10.1038/nmeth.3869

Daims, H., Brühl, A., Amann, R., Schleifer, K. H., & Wagner, M. (1999). The domain-specific probe EUB338 is insufficient for the detection of all bacteria: Development and evaluation of a more comprehensive probe set. *Systematic & Applied Microbiology*, *22*(3), 434–444. https://doi.org/10.1016/s0723-2020(99)80053-8

DeLong, E. F. (1992). Archaea in coastal marine environments. *Proceedings of the National Academy of Sciences of the United States of America*, *89*(12), 5685–5689. https://doi.org/10.1073/pnas.89.12.5685

Fu, Q.-L., Fujii, M., & Riedel, T. (2020). Development and comparison of formula assignment algorithms for ultrahigh-resolution mass Spectra of natural organic matter. *Analytica Chimica Acta*. https://doi.org/10.1016/j.aca.2020.05.048

Gülzow, W., Rehder, G., Deimling, J. S. V., & Sadkowiak, B. (2011). A new method for continuous measurement of methane and carbon dioxide in surface waters using off-axis integrated cavity output spectroscopy (ICOS): An example from the Baltic sea. *Limnology and Oceanography: Methods*, *9*, 176–184. https://doi.org/10.4319/lom.2011.9.176

Herrmann, M., Hädrich, A., & Küsel, K. (2012). Predominance of thaumarchaeal ammonia oxidizer abundance and transcriptional activity in an acidic fen. *Environmental Microbiology*, *14*(11), 3013–3025. https://doi.org/10.1111/j.1462-2920.2012.02882.x

Lewis, E. L., Wallace, D., & Allison, L. J. (1998). *Program developed for CO_2 system calculations Rep*. Brookhaven National Lab., Department of Applied Science and Oak Ridge National Lab., Carbon Dioxide Information Analysis Center.

Loy, A., Lehner, A., Lee, N., Adamczyk, J., Meier, H., Ernst, J., et al. (2002). Oligonucleotide microarray for 16S rRNA gene-based detection of all recognized lineages of sulfate-reducing prokaryotes in the environment. *Applied and Environmental Microbiology*, *68*(10), 5064–5081. https://doi.org/10.1128/aem.68.10.5064-5081.2002

Martin, M. (2011). Cutadapt removes adapter sequences from high-throughput sequencing reads. *EMBnet.journal*, *17*(1). https://doi.org/10.14806/ej.17.1.200

Menzel, P., Ng, K. L., & Krogh, A. (2016). Fast and sensitive taxonomic classification for metagenomics with Kaiju. *Nature Communications*, *7*(1), 11257. https://doi.org/10.1038/ncomms11257

Oksanen, J., Kindt, R., Legendre, P., O'Hara, B., Stevens, M. H. H., Oksanen, M. J., & Suggests, M. A. S. S. (2007). The vegan package: Community ecology package. In *R package version*.

Parada, A. E., Needham, D. M., & Fuhrman, J. A. (2016). Every base matters: Assessing small subunit rRNA primers for marine microbiomes with mock communities, time series and global field samples. *Environmental Microbiology*, *18*(5), 1403–1414. https://doi.org/10.1111/1462-2920.13023

Paulson, J. N., Stine, O. C., Bravo, H. C., & Pop, M. (2013). Differential abundance analysis for microbial marker-gene surveys. *Nature Methods*, *10*(12), 1200–1202. https://doi.org/10.1038/nmeth.2658

Quast, C., Pruesse, E., Yilmaz, P., Gerken, J., Schweer, T., Yarza, P., et al. (2012). The SILVA ribosomal RNA gene database project: Improved data processing and web-based tools. *Nucleic Acids Research*, *41*(D1), D590–D596. https://doi.org/10.1093/nar/gks1219

Quince, C., Lanzen, A., Davenport, R. J., & Turnbaugh, P. J. (2011). Removing noise from pyrosequenced amplicons. *BMC Bioinformatics*, *12*(1), 38. https://doi.org/10.1186/1471-2105-12-38

Röst, H. L., Sachsenberg, T., Aiche, S., Bielow, C., Weisser, H., Aicheler, F., et al. (2016). OpenMS: A flexible open-source software platform for mass spectrometry data analysis. *Nature Methods*, *13*(9), 741–748. https://doi.org/10.1038/nmeth.3959

Takahashi, T., Olafsson, J., Goddard, J. G., Chipman, D. W., & Shutherland, S. (1993). Seasonal variation of CO_2 and nutrients in the high-latitude surface oceans: A comparative study. *Global Biogeochemical Cycles*, *7*, 843–878. https://doi.org/10.1029/93GB02263

Takai, K., & Horikoshi, K. (2000). Rapid detection and quantification of members of the archaeal community by quantitative PCR using fluorogenic probes. *Applied and Environmental Microbiology*, *66*(11), 5066–5072. https://doi.org/10.1128/aem.66.11.5066-5072.2000

Taubert, M., Stöckel, S., Geesink, P., Girnus, S., Jehmlich, N., von Bergen, M., et al. (2018). Tracking active groundwater microbes with D_2O labelling to understand their ecosystem function. *Environmental Microbiology*, *20*(1), 369–384. https://doi.org/10.1111/1462-2920.14010

Van Krevelen, D. (1950). Graphical-statistical method for the study of structure and reaction processes of coal. *Fuel*, *29*, 269–284.

Wang, Q., Garrity, G. M., Tiedje, J. M., & Cole, J. R. (2007). Naive Bayesian classifier for rapid assignment of rRNA sequences into the new bacterial taxonomy. *Applied and Environmental Microbiology*, *73*(16), 5261–5267. https://doi.org/10.1128/aem.00062-07

Wickham, H., François, R., Henry, L., & Müller, K. (2019). *dplyr: a grammar of data manipulation*. R package version.